iScience

CellPress
OPEN ACCESS

Article

CARM1 Regulates AMPK Signaling in Skeletal Muscle

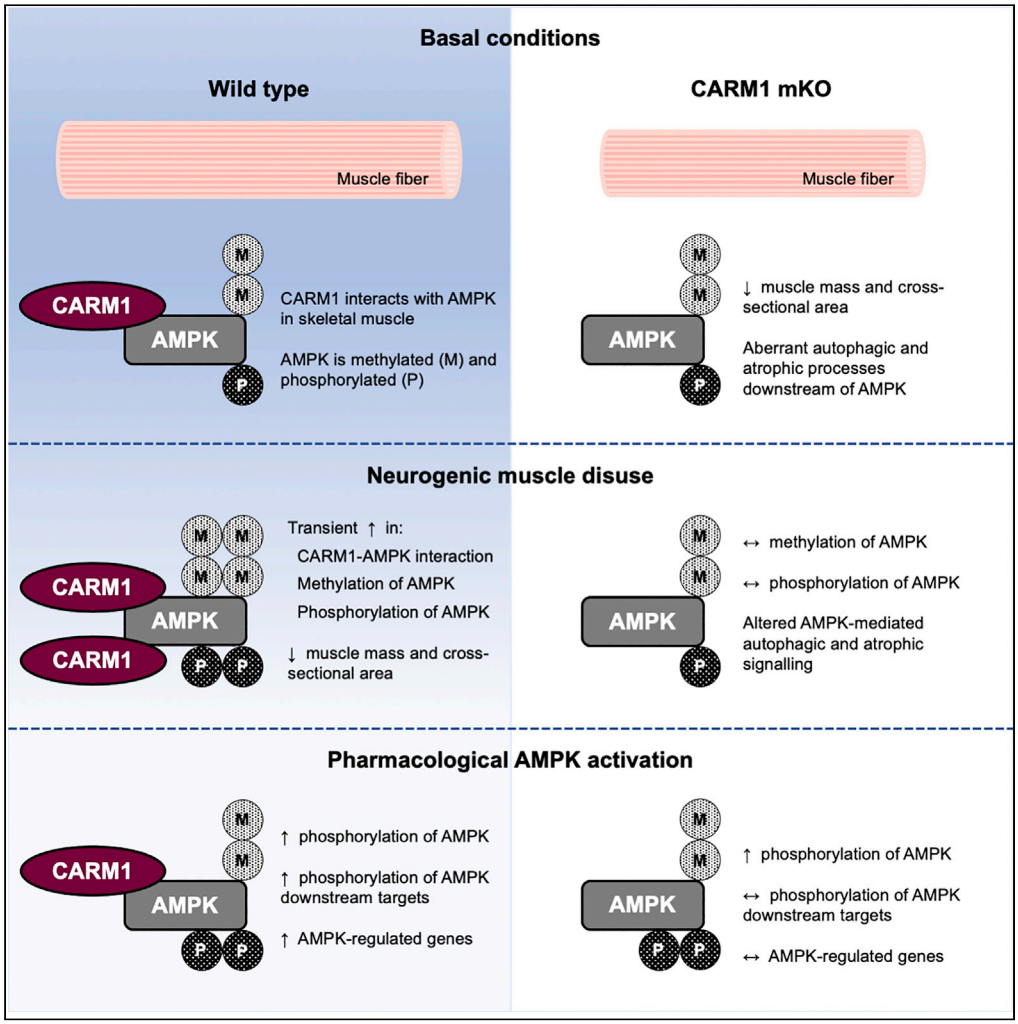

Derek W. Stouth, Tiffany L. vanLieshout, Sean Y. Ng, Erin K. Webb, Alexander Manta, Zachary Moll, Vladimir Ljubicic

ljubicic@mcmaster.ca

HIGHLIGHTS

Role of the arginine methyltransferase CARM1 in muscle biology remains undefined

Skeletal muscle-specific removal of CARM1 alters autophagic and atrophic processes

CARM1 methylates AMPK and mediates AMPK signaling during neurogenic muscle disuse

Targeted pharmacological AMPK stimulation is impacted by CARM1 in skeletal muscle

Stouth et al., iScience *23*, 101755
November 20, 2020
https://doi.org/10.1016/j.isci.2020.101755

iScience

CellPress
OPEN ACCESS

Article

CARM1 Regulates AMPK Signaling in Skeletal Muscle

Derek W. Stouth,[1] Tiffany L. vanLieshout,[1] Sean Y. Ng,[1] Erin K. Webb,[1] Alexander Manta,[1] Zachary Moll,[1] and Vladimir Ljubicic[1,2,*]

SUMMARY

Coactivator-associated arginine methyltransferase 1 (CARM1) is an emerging mediator of skeletal muscle plasticity. We employed genetic, physiologic, and pharmacologic approaches to determine whether CARM1 regulates the master neuromuscular phenotypic modifier AMP-activated protein kinase (AMPK). CARM1 skeletal muscle-specific knockout (mKO) mice displayed reduced muscle mass and dysregulated autophagic and atrophic processes downstream of AMPK. We observed altered interactions between CARM1 and AMPK and its network, including forkhead box protein O1, during muscle disuse. CARM1 methylated AMPK during the early stages of muscle inactivity, whereas CARM1 mKO mitigated progression of denervation-induced atrophy and was accompanied by attenuated phosphorylation of AMPK targets such as unc-51 like autophagy-activating kinase 1^{Ser555}. Lower acetyl-coenzyme A carboxylase^{Ser79} phosphorylation, as well as reduced peroxisome proliferator-activated receptor-γ coactivator-1α, was also observed in mKO animals following acute administration of the direct AMPK activator MK-8722. Our study suggests that targeting CARM1-AMPK interplay may have broad impacts on neuromuscular health and disease.

INTRODUCTION

Coactivator-associated arginine methyltransferase 1 (CARM1) belongs to a family of enzymes known as protein arginine methyltransferases (PRMTs) that catalyze the methylation of arginine residues on target proteins, thereby altering intracellular processes (Bedford and Clarke, 2009; Yang and Bedford, 2013; Guccione and Richard, 2019; Fulton et al., 2019). All nine PRMTs synthesize monomethylarginine (MMA), whereas type I (i.e., PRMT1, PRMT2, PRMT3, CARM1, PRMT6, PRMT8) and type II (i.e., PRMT5, PRMT9) PRMTs deposit asymmetric dimethylarginine (ADMA) and symmetric dimethylarginine (SDMA) marks, respectively, on their target molecules. Arginine methylation is an underappreciated post-translational modification that occurs with the same frequency as the more widely studied and better understood phosphorylation and ubiquitination events (Larsen et al., 2016). CARM1 employs S-adenosyl-L-methionine to methylate arginine residues in proline-rich motifs of histones and non-histone proteins to mediate critical functions such as signal transduction, DNA repair, transcriptional control, mRNA splicing, and protein translocation (Bedford and Clarke, 2009; Yang and Bedford, 2013; Guccione and Richard, 2019; Fulton et al., 2019). For instance, CARM1 methylates histone H3 at Arg17 and co-activates transcription factor EB (TFEB) to promote the expression of autophagy-related genes (Shin et al., 2016). CARM1 is ubiquitously expressed, and whole-body genetic deletion of this enzyme in mice results in perinatal lethality (Yadav et al., 2003).

CARM1 has emerged as an important player in skeletal muscle biology. Work from our laboratory indicates that the methyltransferase is a novel regulator of skeletal muscle remodeling in rodents and humans (Ljubicic et al., 2012; Stouth et al., 2017, 2018; Vanlieshout et al., 2018; Shen et al., 2018; vanLieshout and Ljubicic, 2019; vanLieshout et al., 2019). Moreover, a series of elegant studies demonstrate that CARM1 governs myogenesis during development and regeneration, as well as plays a role in muscle glycogen metabolism (Chen et al., 2002; Kawabe et al., 2012; Wang et al., 2012; Chang et al., 2018). Recent data strongly suggest that CARM1 also impacts atrophy and autophagy signaling in muscle. For example, transient knockdown of CARM1 during denervation-induced muscle disuse attenuated the progression of muscle wasting and the expression of the atrophy-related genes via a forkhead box protein O3 (FOXO3)-mediated mechanism (Liu et al., 2019). In an earlier study, we reported that denervation-induced skeletal muscle atrophy was associated with elevated CARM1 expression and arginine methyltransferase activity, as well as

[1]Department of Kinesiology, McMaster University, Hamilton, ON L8S 4L8, Canada

[2]Lead Contact

*Correspondence: ljubicic@mcmaster.ca

https://doi.org/10.1016/j.isci.2020.101755

increased AMP-activated protein kinase (AMPK) activation status (Stouth et al., 2018). AMPK is a master regulator of phenotype determination, maintenance, and plasticity in skeletal muscle (Mounier et al., 2015; Dial et al., 2018; Kjøbsted et al., 2018; Steinberg and Carling, 2019). Notably, AMPK promotes autophagy in skeletal muscle through direct activation of unc-51-like autophagy-activating kinase 1 (ULK1) and FOXO3 (Kjøbsted et al., 2018). AMPK also upregulates atrogenes that drive the ubiquitin-proteasome system such as muscle RING finger 1 (MuRF1) and muscle atrophy F box (MAFbx) during muscle disuse (Kjøbsted et al., 2018). Thus, this collective evidence highlights the roles of CARM1 and AMPK in the orchestration of skeletal muscle remodeling via regulation of autophagy-lysosome and ubiquitin-proteasome signaling pathways.

Recent studies using non-muscle cells directly link CARM1 with AMPK and suggest that these molecules work synergistically to govern autophagic and atrophic networks (Shin et al., 2016; Kim et al., 2014). For instance, under nutrient-deprived conditions, AMPK-dependent phosphorylation of FOXO3 led to increased CARM1 expression and activity levels coincident with the stimulation of pro-autophagic signaling (Shin et al., 2016). In turn, CARM1 induced TFEB, the master transcriptional regulator of the autophagy program. The relationship between CARM1 and AMPK in skeletal muscle is less understood (Ljubicic et al., 2012; Stouth et al., 2018), but may represent a novel, powerful nexus for control of phenotypic plasticity in this tissue. Therefore, in the present study, we employed a combination of genetic, physiologic, and pharmacologic approaches to test the hypothesis that CARM1 interacts with AMPK to affect the kinase's downstream signaling network and muscle phenotype.

RESULTS

Generation of CARM1 Skeletal Muscle-Specific Knockout (mKO) Mice

To examine the function of CARM1 in muscle, we utilized the Cre/*loxP* system to generate mice that lack the enzyme specifically in skeletal muscle (Figure 1A). CARM1 floxed animals (Yadav et al., 2003; Bao et al., 2018) were bred to mice that expressed Cre recombinase under control of the human α-skeletal actin promoter, the activity of which is restricted to skeletal muscle tissue (McCarthy et al., 2012). A significant main effect of genotype was noted on CARM1 transcript levels and a significant interaction between genotype and muscle was also observed (Figure 1B). We found ∼90%–95% lower ($p < 0.05$) CARM1 transcript levels in mKO mice versus their wild-type (WT) littermates in both fast, glycolytic extensor digitorum longus (EDL) muscle and slower, more oxidative soleus (SOL) muscle. Relative to the WT EDL, CARM1 mRNA content was significantly lower by ∼13% in the WT SOL. Immunoblot analyses confirmed that CARM1 protein expression was significantly reduced in various skeletal muscles from mKO mice (Figure 1C). There was a trend ($p = 0.46$) for lower CARM1 protein content in the SOL versus tibialis anterior (TA), EDL, and gastrocnemius (GAST) muscles in WT animals (Figure 1D). CARM1 protein levels were similar between genotypes in other tissues such as the liver and brain (Figure 1E). Furthermore, CARM1 protein expression was similar in WT versus mKO heart muscles (Figures 1F and 1G). Compared with their WT littermates, the average body mass of mKO mice was modestly, but significantly, lower (∼5%; Figure 1H). Heart weights expressed relative to body mass were also similar in WT versus mKO animals (Figure 1I).

CARM1 Deletion in Skeletal Muscle Mitigates Denervation-Induced Atrophy

We previously reported elevated CARM1 expression and methyltransferase activity in response to 3 and 7 days of neurogenic muscle disuse (Stouth et al., 2018). Moreover, transient knockdown of CARM1 in TA muscle blunted the progression of muscle wasting after 4 weeks of denervation (Liu et al., 2019). However, the function of CARM1 during neurogenic muscle disuse remains to be fully understood. As such, we assessed physiological and mechanistic effects of denervation-induced muscle disuse in CARM1 mKO animals. As the average body mass was different between genotypes (Figure 1H), muscle was normalized to total body mass for subsequent analyses. After 3 days of neurogenic disuse elicited by unilateral sciatic nerve transection, a main effect ($p < 0.05$) of denervation on SOL muscle mass was observed in both genotypes (Figure 2A). Indeed, when compared with the contralateral, non-denervated CON limb, SOL muscle mass was significantly reduced by ∼25% and ∼15% in WT and mKO animals, respectively, in the DEN limb after 3 days. We also detected a main effect ($p < 0.05$) of genotype on SOL muscle mass following 3 days of denervation. Relative to the CON limb, TA and GAST muscle mass were significantly lower in WT animals by ∼15% after 3 days in the DEN limb. In contrast, TA and GAST muscle mass were similar between CON and DEN limbs in mKO animals following 3 days of disuse. EDL muscle mass did not differ between CON and DEN limbs in WT and mKO mice after 3 days. In response to 7 days of unilateral hindlimb disuse, we observed a statistical interaction between genotype and treatment (i.e., denervation) for EDL muscle

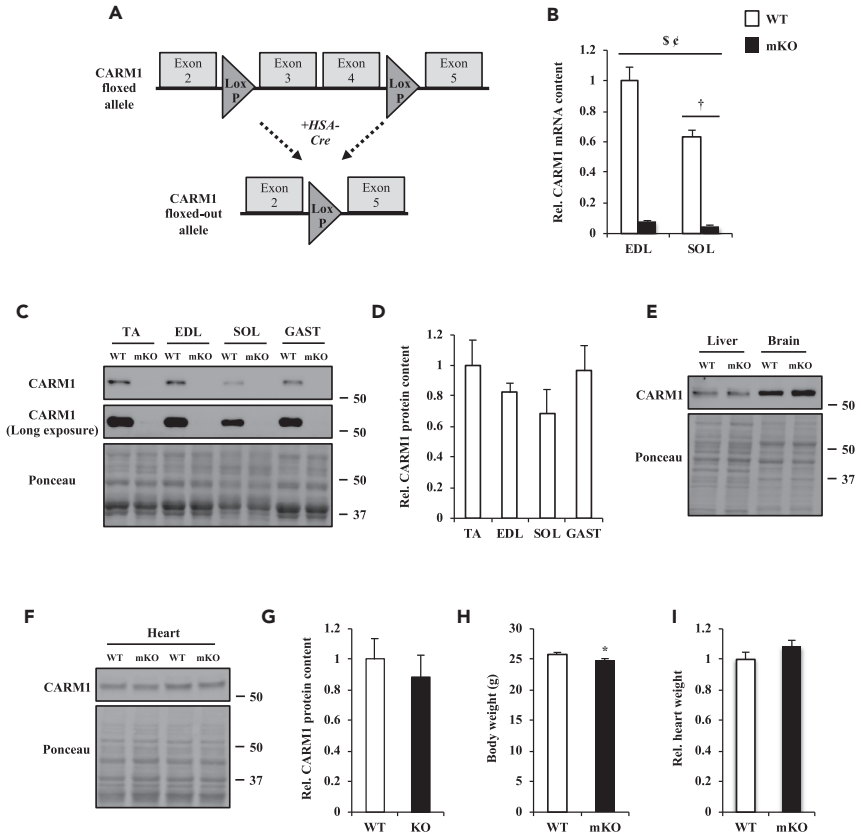

Figure 1. Generation of Skeletal Muscle-Specific Coactivator-Associated Arginine Methyltransferase 1 (CARM1) Knockout (mKO) Mice

(A) Simplified schematic of floxed exon 3 and exon 4 of the CARM1 gene with arrows to indicate deletion by human α-skeletal actin (*HSA*)-driven Cre-recombinase in skeletal muscle.

(B) CARM1 mRNA expression in extensor digitorum longus (EDL) and soleus (SOL) muscles of wild-type (WT) and CARM1 mKO mice. Data are expressed relative to the WT EDL muscle (n = 9–12).

(C) Representative western blots of CARM1 protein content (normal and long exposures) in the tibialis anterior (TA), EDL, SOL, and gastrocnemius (GAST) muscles from WT and mKO mice, as well as a representative Ponceau stain, below. Molecular weights (kDa) are shown at right of blots.

(D) Graphical summary of CARM1 protein expression in TA, EDL, SOL, and GAST muscles of WT animals. Data are expressed as protein content relative to WT TA (n = 9–11).

(E) CARM1 protein content in the liver and brain, along with a typical Ponceau stain. Molecular weights (kDa) are shown on the right (n = 3).

(F) Representative western blot of CARM1 protein content in heart muscles from WT and mKO animals, as well as a representative Ponceau stain, below. Molecular weights (kDa) are shown at the right of blots.

(G) Graphical summary of CARM1 protein expression in heart muscles of WT and mKO animals. Data are expressed as protein content relative to WT heart (n = 14–15).

(H) Body mass of WT and mKO animals (n = 44–51).

(I) Heart weight expressed relative to body mass in WT and mKO mice (n = 12).

Data are expressed relative to the WT value. Data are means ± SEM. Student's t test; *$p < 0.05$ versus WT. Two-way ANOVA; $$p < 0.05$ interaction effect of genotype and muscle; ¢$p < 0.05$ main effect of genotype; †$p < 0.05$ main effect of muscle.

mass (Figure 2B). Tukey post-hoc analyses revealed that EDL and GAST muscle mass were significantly lower by ~40% and ~30% in the DEN limb, respectively, relative to the CON limb after 7 days in WT mice. However, EDL and GAST muscle weights did not differ between CON and DEN limbs in mKO animals. A main effect ($p < 0.05$) of denervation on TA and SOL muscle mass was observed after 7 days of neurogenic disuse. Relative to the CON limb, TA and SOL muscle weights were significantly lower by ~25%–30% and ~40%–45%, respectively, after 7 days in the DEN limbs of WT and mKO mice. A significant main effect of genotype on TA muscle mass was also detected after 7 days.

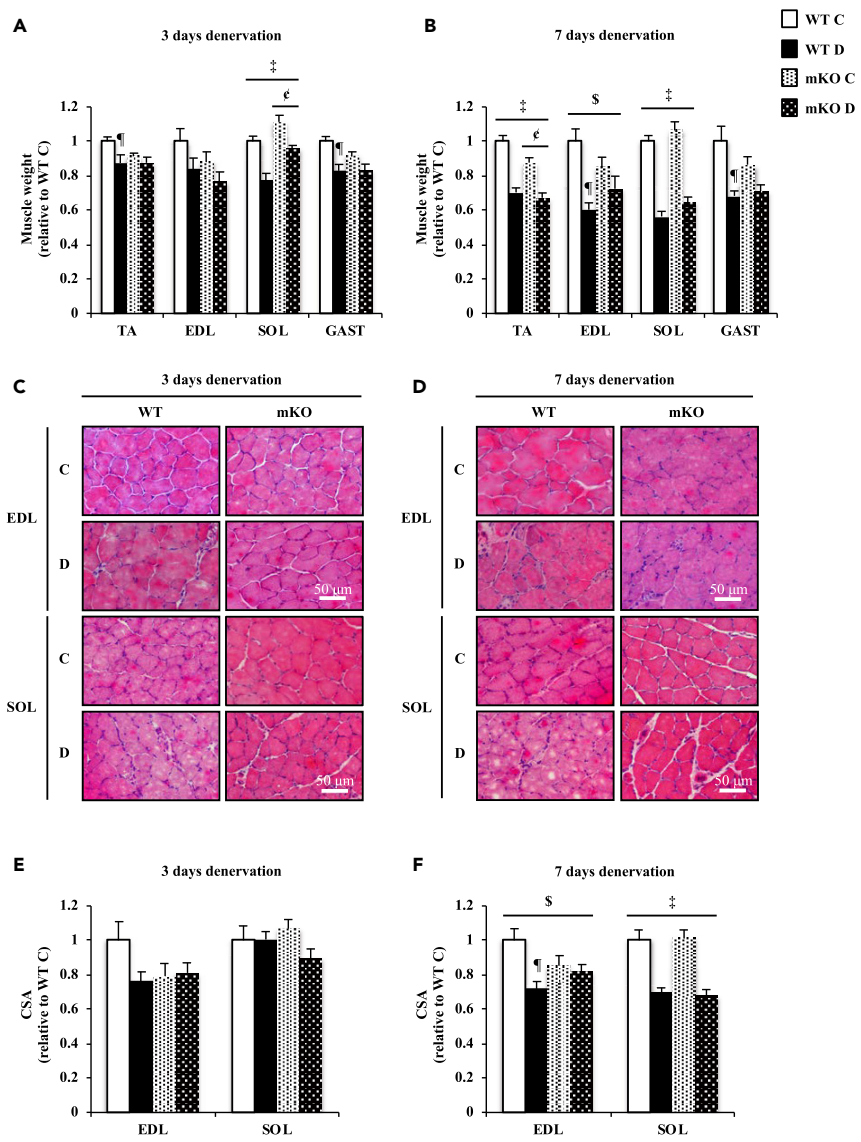

Figure 2. CARM1 Deletion in Skeletal Muscle Mitigates Denervation-Induced Atrophy

TA, EDL, SOL, and GAST muscle mass from the denervated (D) and the contralateral, non-denervated control (C) hindlimbs of WT and mKO mice after 3 (A) and 7 (B) days of denervation. Muscle weights are normalized to body weight, and data are expressed as muscle mass relative to WT C (n = 8–17). Representative images of H&E-stained EDL and SOL muscle cross sections from WT and mKO mice in D and C hindlimbs following 3 (C) and 7 (D) days of denervation. Scale bar, 50 µm. Graphical summaries of the average myofiber cross-sectional area (CSA) of EDL and SOL muscles from WT and mKO mice in D and C hindlimbs after 3 (E) and 7 (F) days of neurogenic muscle disuse. Data are expressed as CSA relative to the WT C (n = 5–9). Data are means ± SEM. Two-way ANOVA; $p < 0.05 interaction effect of genotype and denervation; ¢p < 0.05 main effect of genotype; ‡p < 0.05 main effect of denervation; ¶p < 0.05 versus WT C.

EDL and SOL myofiber cross-sectional area (CSA) was similar between CON and DEN limbs in WT and mKO animals following 3 days of neurogenic muscle disuse (Figures 2C and 2E). However, an interaction ($p < 0.05$) between genotype and denervation for EDL CSA emerged after 7 days (Figures 2D and 2F). Relative to CON, denervation induced a 28% decrease ($p < 0.05$) in EDL CSA in WT animals that was abolished in the absence of CARM1. Moreover, a significant main effect of denervation on SOL CSA was observed in both genotypes following 7 days of unilateral disuse. For instance, when compared with the CON limbs, SOL CSA was significantly reduced by ~30% in the DEN limbs of WT and mKO mice.

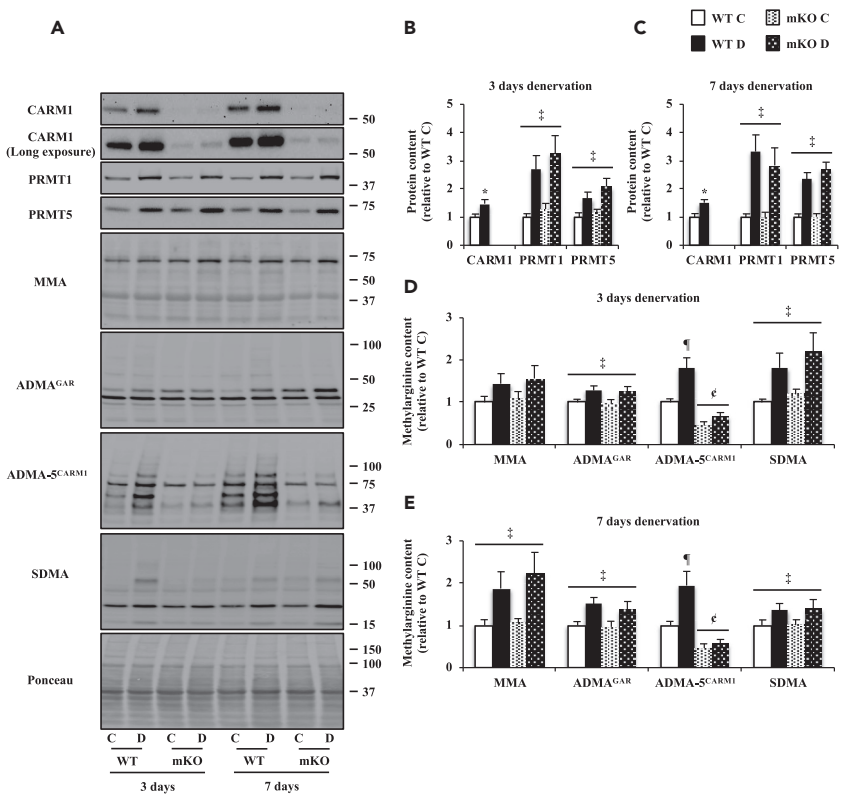

Figure 3. Skeletal Muscle Protein Arginine Methyltransferase (PRMT) Content and Activity Are Elevated in mKO Mice during Neurogenic Disuse

(A) Representative western blots of CARM1 (normal and long exposure), PRMT1, PRMT5, monomethylarginine (MMA), asymmetric dimethylarginine (ADMA) at glycine and arginine-rich motifs (ADMA^{GAR}), ADMA-CARM1 motif (ADMA-5^{CARM1}), and symmetric dimethylarginine (SDMA) levels in C and D TA muscles after 3 and 7 days of unilateral denervation in WT and mKO mice, with a typical Ponceau stain. Molecular weights (kDa) are shown at the right of blots. Graphical summaries of CARM1, PRMT1, and PRMT5 protein expression in TA muscles from the C and D hindlimbs of WT and mKO animals following 3 (B) and 7 (C) days of denervation. Data are expressed as protein content relative to WT C (n = 8–10). Graphical summaries of MMA, ADMA^{GAR}, ADMA-5^{CARM1}, and SDMA methylarginine content in C and D TA muscles of WT and mKO mice after 3 (D) and 7 (E) days. Data are expressed as methylarginine content relative to WT C (n = 6–10). Data are means ± SEM. Student's t test; *$p < 0.05$ versus WT C. Two-way ANOVA; \$$p < 0.05$ interaction effect of genotype and denervation; ¢$p < 0.05$ main effect of genotype; ‡$p < 0.05$ main effect of denervation; ¶$p < 0.05$ versus WT C.

Skeletal Muscle PRMT Content and Activity Are Elevated in mKO Mice during Neurogenic Disuse

CARM1 protein content was elevated by ~1.5-fold ($p < 0.05$) in DEN versus CON WT limbs following 3 and 7 days of neurogenic muscle disuse (Figures 3A–3C). We wished to determine whether knocking out CARM1 in skeletal muscle elicited adaptations in other PRMTs after denervation. Thus, we examined PRMT1 and PRMT5 protein expression in the TA muscle of mKO animals, as well as markers of type I and type II PRMT activities, such as MMA, ADMA at glycine and arginine-rich motifs (ADMA^{GAR}), and SDMA (Bedford and Clarke, 2009; Yang and Bedford, 2013). We also probed for pan-CARM1-marked substrates (ADMA-5^{CARM1}; Cheng et al. 2018; vanLieshout et al., 2019). A main effect ($p < 0.05$) of denervation on PRMT1 and PRMT5 protein levels was observed in both genotypes after 3 and 7 days (Figures 3A–3C). PRMT1 and PRMT5 expression levels were significantly greater by ~2.5- to 3.3-fold and ~1.7- to 2.6-fold, respectively, in DEN versus CON limbs in WT and mKO mice.

A significant main effect of denervation on ADMA^{GAR} and SDMA content was observed in both genotypes following 3 and 7 days (Figures 3A, 3D, and 3E). Moreover, we detected a main effect ($p < 0.05$) of denervation on MMA content in WT and mKO animals after 7 days. ADMA-5^{CARM1} exhibited a trend toward a

statistically significant interaction between genotype and denervation after 3 and 7 days ($p = 0.08$ and $p = 0.06$, respectively). Specifically, relative to the CON limb, neurogenic muscle disuse induced a significant 1.8- and 1.9-fold increase in ADMA-5^{CARM1} content in the DEN limb after 3 and 7 days, respectively, in WT mice. ADMA-5^{CARM1} did not differ between CON and DEN limbs after 3 and 7 days of denervation in mKO animals. Furthermore, a significant main effect of genotype on ADMA-5^{CARM1} content was detected following 3 and 7 days.

Signaling Molecules That Regulate Skeletal Muscle Remodeling Are Altered in Response to Denervation

We next sought to determine whether CARM1 influences powerful modifiers of skeletal muscle phenotype such as AMPK, peroxisome proliferator-activated receptor-γ coactivator-1α (PGC-1α), tumor-suppressor protein p53, silent mating-type information regulator 2 homolog 1 (SIRT1), mitochondrial transcription factor A (Tfam), and nuclear factor erythroid 2-related factor 2 (Nrf2; Ljubicic et al., 2014; Dial et al., 2018; Hood et al., 2019). To this end, we first examined the activation status (i.e., the phosphorylated form of the protein relative to its total, unphosphorylated content) of AMPK and its target acetyl-coenzyme A carboxylase (ACC), as well as the protein content of downstream phenotypic modifiers PGC-1α and p53 in the TA muscle of WT and mKO animals subjected to denervation. We also assessed SIRT1, PGC-1α, p53, Tfam, and Nrf2 transcript levels in the EDL muscle following neurogenic muscle disuse. A significant interaction between genotype and denervation for phosphorylated AMPK (P-AMPK)^{Thr172} was observed after 3 days of neurogenic muscle disuse in the TA muscle (Figures 4A and 4B). For example, relative to the CON limb, P-AMPK^{Thr172} content in WT animals was significantly greater by 1.8-fold after 3 days in the DEN limb, whereas the phosphorylation of AMPK^{Thr172} did not differ between CON and DEN limbs following 3 days of denervation in mKO animals. In contrast, there were no significant differences for P-AMPK^{Thr172} levels between CON and DEN limbs in WT and mKO mice after 7 days of disuse. Notably, a significant main effect of genotype on P-AMPK^{Thr172} content was detected after 3 days (Figures 4A and 4C). Neither genotype nor denervation had an effect on total AMPK content following 3 and 7 days. An interaction ($p < 0.05$) between genotype and denervation for AMPK activation status was observed after 3 days, along with a significant main effect of genotype. The activation status for AMPK did not differ between CON and DEN limbs in WT and mKO animals following 7 days. A main effect ($p < 0.05$) of genotype on ACC^{Ser79} phosphorylation was observed after 3 days of denervation, along with a trend ($p = 0.06$) toward a main effect of genotype following 7 days (Figures 4A, 4D, and 4E). Total ACC content was similar between CON and DEN limbs in WT and mKO mice after 3 and 7 days of neurogenic muscle disuse. A significant main effect of genotype was detected for ACC activation status following 3 and 7 days. A notable main effect ($p < 0.05$) of denervation was apparent for ACC activation status after 3 days of denervation.

We observed a main effect ($p < 0.05$) of genotype on PGC-1α protein content in TA muscles after 3 and 7 days (Figures 4A, 4F, and 4G). Moreover, a main effect ($p < 0.05$) of denervation on PGC-1α protein expression was detected in both genotypes following 7 days. We observed a significant main effect of denervation on p53 protein content (+3.2-fold) in WT mice after 7 days (Figures 4A and 4G). In contrast, p53 protein levels did not differ between CON and DEN limbs in mKO animals after 7 days of denervation. PGC-1α and p53 stimulate mitochondrial biogenesis in skeletal muscle (Ljubicic et al., 2014; Hood et al., 2019). Thus, we next assessed the expression of protein subunits that are representative of mitochondrial oxidative phosphorylation (OXPHOS) complexes I–V (CI–CV), as well as succinate dehydrogenase (SDH) content in WT and mKO animals. We detected a main effect ($p < 0.05$) of denervation on total OXPHOS expression in both genotypes after 3 and 7 days of denervation (Figures 4A, 4F, and 4G). Qualitative analyses suggest that compared with the control limbs, both WT and mKO EDL muscles displayed reduced SDH staining after 7 days of neurogenic muscle disuse (Figure 4H).

Denervation did not have an effect on SIRT1 mRNA content following 3 or 7 days in the EDL muscle (Figures 4I and 4J). A main effect ($p < 0.05$) of denervation on PGC-1α mRNA expression was observed in both genotypes after 3 and 7 days in the EDL muscles. PGC-1α was significantly lower by ~57%–87% in DEN versus CON limbs in WT and mKO mice (Figures 4I and 4J). An interaction ($p < 0.05$) between genotype and denervation for p53 transcript levels in the EDL muscle emerged after 3 days (Figure 4I). Relative to CON, denervation induced a 3.2-fold increase in p53 mRNA expression in the WT EDL ($p < 0.05$) that was blunted in the absence of CARM1. A significant main effect of denervation on EDL p53 transcript levels was observed in both genotypes after 7 days (Figure 4J). Specifically, when compared with the CON limb, p53 mRNA content was significantly elevated by ~1.8- to 2.2-fold in the DEN EDL following 7 days. We detected a main

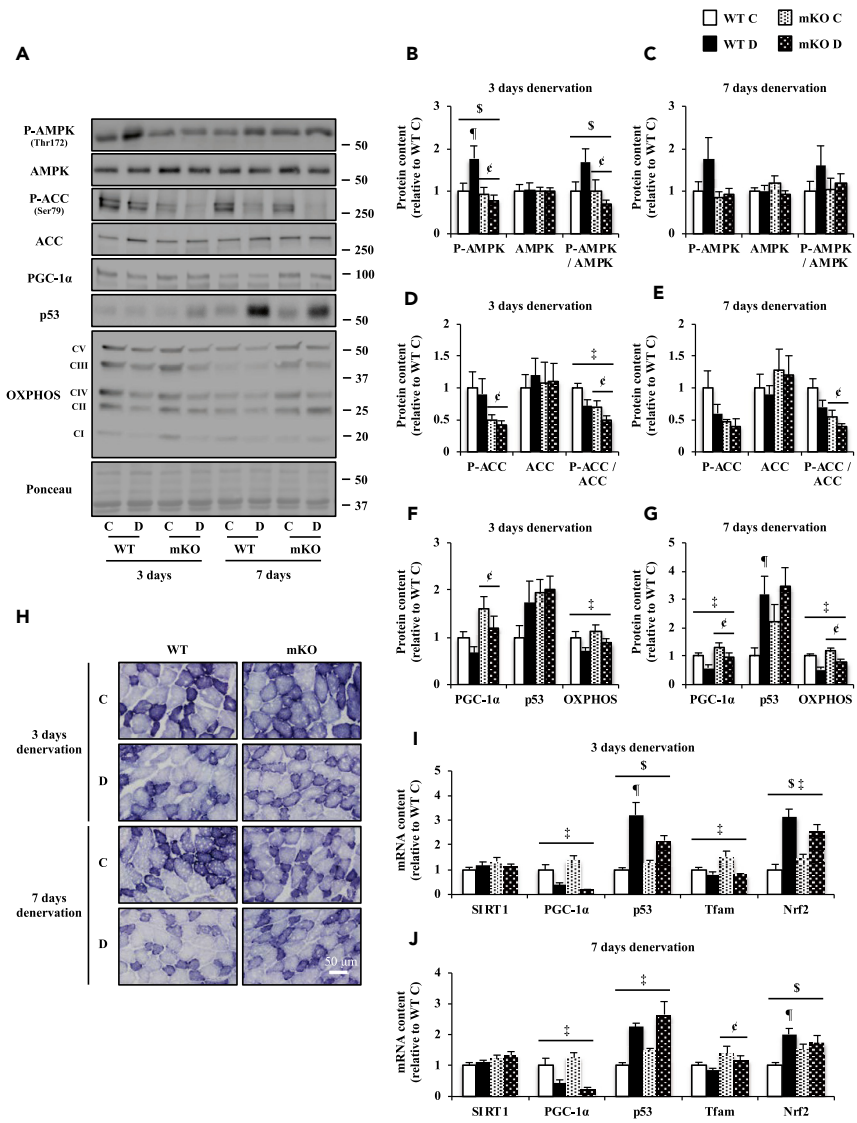

Figure 4. Signaling Molecules That Regulate Skeletal Muscle Remodeling Are Altered in Response to Denervation

(A) Representative western blots of phosphorylated AMP-activated protein kinase (P-AMPK)^{Thr172}, total AMPK, phosphorylated acetyl-coenzyme A carboxylase (P-ACC)^{Ser79}, total ACC, peroxisome proliferator-activated receptor-γ coactivator-1α (PGC-1α), tumor suppressor protein p53 protein content, and proteins indicative of mitochondrial oxidative phosphorylation (OXPHOS) complexes I–V (CI–CV) in C and D TA muscles following 3 and 7 days of unilateral denervation in WT and mKO mice, accompanied by a typical Ponceau stain. Molecular weights (kDa) are shown at the right of blots.

(B–G) Graphical summaries of P-AMPK^{Thr172}, AMPK, AMPK activation status (i.e., the phosphorylated form of the protein relative to the total amount of the protein), P-ACC^{Ser79}, ACC, ACC activation status, PGC-1α, p53, and total OXPHOS protein expression in the C and D TA muscles of WT and mKO mice following 3 and 7 days of neurogenic disuse. Data are expressed as protein content relative to WT C (n = 5–11).

(H) Representative images of succinate dehydrogenase (SDH)-stained EDL muscle cross-sections from WT and mKO mice in D and C hindlimbs following 3 and 7 days of denervation. Scale bar, 50 μm (n = 3–5). Silent mating-type information regulator 2 homolog 1 (SIRT1), PGC-1α, p53, mitochondrial transcription factor A (Tfam), and nuclear factor erythroid 2-related factor 2 (Nrf2) mRNA expression in EDL muscles from the C and D hindlimbs of WT and mKO animals after 3 (I) and 7 (J) days of denervation. Data are expressed as mRNA content relative to WT C (n = 4–8). Data are means ± SEM. Two-way ANOVA; $p < 0.05 interaction effect of genotype and denervation; ¢p < 0.05 main effect of genotype; ‡p < 0.05 main effect of denervation; ¶p < 0.05 versus WT C.

effect ($p < 0.05$) of denervation on Tfam mRNA expression following 3 days of disuse (Figure 4I). Most notable was the significant decline in Tfam mRNA content by ~49% in the DEN versus CON EDL in mKO mice. A main effect ($p < 0.05$) of genotype on Tfam transcript levels was also observed after 7 days (Figure 4J). Statistically significant interactions between genotype and denervation for Nrf2 mRNA levels were observed after 3 and 7 days (Figures 4I and 4J). Following 3 days, Nrf2 mRNA expression in WT and mKO mice was significantly increased by 3.1- and 1.8-fold, respectively, in the DEN versus CON EDL muscles. Relative to CON, denervation induced a 2-fold increase ($p < 0.05$) in Nrf2 mRNA content in WT EDL after 7 days that was abolished in the absence of CARM1.

CARM1 Influences the Muscle Atrophy Program during Neurogenic Muscle Disuse

To examine the impact of CARM1 on the muscle atrophy program, we assessed markers of the autophagy-lysosome pathway and the ubiquitin-proteasome system in WT and mKO animals after disuse. Specifically, we evaluated markers of autophagosome formation such as phosphorylation of ULK1^{Ser555} and lipidation of microtubule-associated protein 1A/1B-light chain 3 (LC3; i.e., the conversion of nonlipidated LC3-I to lipidated LC3-II; Vainshtein et al., 2014). We also analyzed the activation status of FOXO1^{Ser256} and FOXO3^{Ser588} as FOXO1 and FOXO3 regulate the transcription of atrogenes important for proteasome-mediated degradation (Bodine, 2013). The phosphorylation of ULK1^{Ser555} exhibited a trend ($p = 0.14$) toward an interaction between genotype and denervation after 3 days of disuse (Figures 5A and 5B). Relative to the CON limb, P-ULK1^{Ser555} content in WT mice was significantly greater by 1.7-fold following 3 days in the DEN limb, whereas the phosphorylation of ULK1^{Ser555} did not differ between CON and DEN limbs after 3 days of neurogenic muscle disuse in mKO animals. In contrast, similar P-ULK1^{Ser555} levels were detected between CON and DEN limbs in WT and mKO mice after 7 days of disuse (Figures 5A and 5C). Total ULK1 did not differ between CON and DEN limbs following 3 and 7 days of denervation in WT and mKO animals (Figures 5A–5C). The activation status for ULK1 was also similar between CON and DEN limbs in WT and mKO animals following 3 and 7 days. A main effect ($p < 0.05$) of denervation on the phosphorylation of FOXO1^{Ser256} was observed in WT animals after 3 days of disuse in TA muscles (Figures 5A and 5D). We also detected a significant main effect of denervation on the phosphorylation of FOXO1^{Ser256} in both genotypes following 7 days (Figures 5A and 5E). The phosphorylation of FOXO1^{Ser256} was greater by ~1.4- to 2.1-fold in DEN versus CON limbs in WT and mKO mice after denervation. A significant main effect of denervation on total FOXO1 content was observed in both genotypes following 3 days. Relative to the CON limb, neurogenic muscle disuse induced a ~2.1–2.6-fold increase in FOXO1 content in WT and mKO mice. A main effect ($p < 0.05$) of genotype on total FOXO1 protein expression was also detected following 3 days. A significant main effect of denervation on total FOXO1 content was apparent in WT animals following 7 days. A main effect ($p < 0.05$) of denervation on FOXO1 activation status was observed in both genotypes after 3 days. FOXO1 activation status did not differ between CON and DEN limbs following 7 days of denervation in WT and mKO animals. An interaction ($p < 0.05$) between genotype and denervation for the phosphorylation of FOXO3^{Ser588} emerged after 3 days of denervation (Figures 5A and 5F). Moreover, a significant main effect of genotype on FOXO3^{Ser588} phosphorylation was observed in both genotypes following 3 and 7 days of unilateral disuse (Figures 5A, 5F, and 5G). We detected a main effect ($p < 0.05$) of denervation on total FOXO3 content after 3 days. A significant main effect of genotype on FOXO3 activation status was also observed following 3 and 7 days of neurogenic muscle disuse.

We continued to probe the impact of CARM1 on the muscle atrophy program by analyzing atrogenes that are critically important for muscle wasting. Thus, we assessed the protein expression of p62, Beclin1, TFEB, MuRF1, ubiquitinated protein content, as well as LC3-I and LC3-II expression levels in TA muscles from WT and mKO animals following neurogenic muscle disuse (Hood et al., 2019; Vainshtein et al., 2014; Bodine, 2013; Sandri, 2013). A main effect ($p < 0.05$) of denervation on p62, MuRF1, and ubiquitinated protein content was observed in both genotypes following 3 and 7 days of unilateral disuse (Figures 5A, 5H, and 5I). Relative to the CON limb, p62, MuRF1, and ubiquitinated protein content was significantly greater by ~1.7- to 2.9-fold in the DEN limbs of WT and mKO mice. A main effect ($p < 0.05$) of genotype on ubiquitinated protein content was observed after 3 days. Beclin1 and TFEB protein expression levels were not impacted by disuse. A significant main effect of genotype on Beclin1 protein content was observed following 3 and 7 days of denervation. We found a main effect ($p < 0.05$) of denervation on LC3-I (data not shown) and LC3-II content in both genotypes after 7 days (Figures 5A and 5I). For instance, LC3-I and LC3-II expression levels were significantly greater by ~3.3- to 4.4-fold in the DEN limb relative to the CON limb after 7 days in WT and mKO mice. A main effect ($p < 0.05$) of genotype on LC3-II protein content was also detected after 7 days.

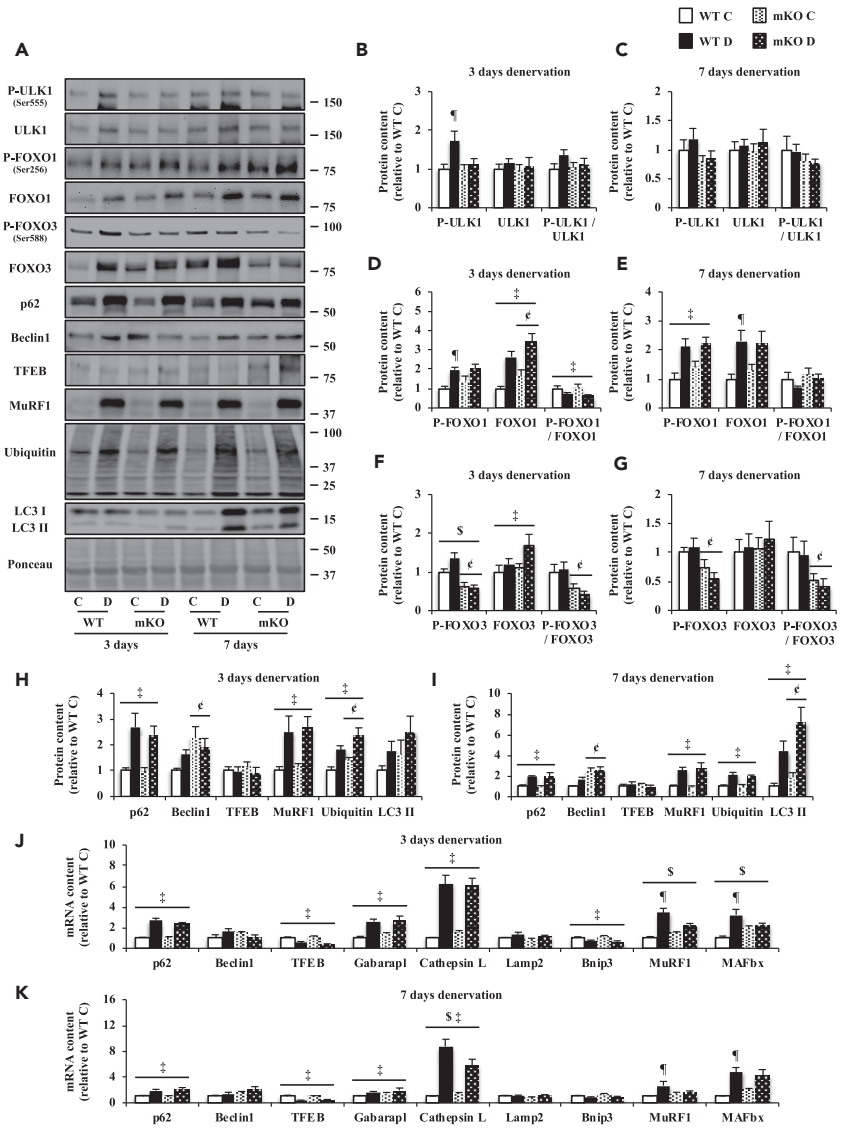

Figure 5. CARM1 Influences the Muscle Atrophy Program during Neurogenic Muscle Disuse

(A) Representative western blots of phosphorylated unc-51 like autophagy-activating kinase 1 (P-ULK1)^{Ser555}, total ULK1, phosphorylated Forkhead box O1 (P-FOXO1)^{Ser256}, total FOXO1, P-FOXO3^{Ser588}, total FOXO3, p62, Beclin1, transcription factor EB (TFEB), muscle RING finger 1 (MuRF1), ubiquitin protein content, microtubule-associated protein 1A/1B-light chain 3 (LC3)-I, and LC3-II in C and D TA muscles following 3 and 7 days of unilateral denervation in WT and mKO mice, accompanied by a typical Ponceau stain. Molecular weights (kDa) are shown on the right of blots.

(B–I) Graphical summaries of P-ULK1^{Ser555}, ULK1, ULK1 activation status, P-FOXO1^{Ser256}, FOXO1, FOXO1 activation status, P-FOXO3^{Ser588}, FOXO3, FOXO3 activation status, as well as p62, Beclin1, TFEB, MuRF1, ubiquitin, and LC3-II protein content in the C and D TA muscles of WT and mKO animals after 3 and 7 days of neurogenic disuse. Data are expressed as protein content relative to WT C (n = 5–11). p62, Beclin1, TFEB, Gabarapl, Cathepsin L, lysosomal-associated membrane protein 2 (Lamp2), BCL2 and adenovirus E1B 19-kDa interacting protein 3 (Bnip3), MuRF1, and muscle atrophy F box (MAFbx) mRNA expression in EDL muscles from the C and D hindlimbs of WT and mKO mice following 3 (J) and 7 (K) days of denervation. Data are expressed as mRNA content relative to WT C (n = 4–8). Data are means ± SEM. Two-way ANOVA; $p < 0.05 interaction effect of genotype and denervation; ¢p < 0.05 main effect of genotype; ‡p < 0.05 main effect of denervation; ¶p < 0.05 versus WT C.

We sought to investigate the effect of CARM1 deletion on the expression of a broad panel of representative atrogenes. To this end, we examined p62, Beclin1, TFEB, Gabarapl, Cathepsin L, lysosomal-associated membrane protein 2 (Lamp2), BCL2, and adenovirus E1B 19-kDa-interacting protein 3 (Bnip3), MuRF1, and

MAFbx transcript levels in EDL muscles from WT and mKO mice. A main effect ($p < 0.05$) of denervation on p62, Gabarapl, and TFEB transcript levels for WT and mKO animals was observed in the EDL muscles after 3 and 7 days of neurogenic muscle disuse (Figures 5J and 5K). In particular, relative to the CON limb, p62 mRNA expression was significantly greater by ~1.9- to 2.7-fold in the DEN EDL muscle in both genotypes. Denervation induced a ~1.9- to 2.6-fold increase ($p < 0.05$) in Gabarapl mRNA content in WT and mKO EDL muscles following 3 days. In contrast, TFEB mRNA content in both genotypes was significantly lower by ~47%–63% in the DEN versus CON EDL after 3 and 7 days. A main effect ($p < 0.05$) of denervation on Bnip3 transcript levels was detected in mKO animals following 3 days. In particular, Bnip3 mRNA expression was lower by ~44% ($p < 0.05$) in mKO animals in the DEN versus CON EDL. Statistically significant interactions between genotype and denervation for Cathepsin L, MuRF1, and MAFbx transcript levels were also observed (Figures 5J and 5K). Specifically, in EDL muscles of DEN versus CON limbs, denervation induced a ~2.7- to 4.7-fold increase ($p < 0.05$) in MuRF1 and MAFbx transcripts in WT animals after 3 and 7 days, whereas no significant changes were observed in the absence of CARM1. An interaction ($p < 0.05$) between genotype and denervation for Cathepsin L transcript levels in the EDL emerged after 7 days (Figure 5K). Relative to the WT CON EDL muscle, denervation induced a ~8.8-fold increase ($p < 0.05$) in Cathepsin L mRNA expression in the WT EDL that was blunted (~3.8-fold) in mKO animals. Beclin1 and Lamp2 mRNA transcripts in the EDL muscles did not differ between CON and DEN limbs following disuse (Figures 5J and 5K).

CARM1 Interacts with AMPK, FOXO1, and TFEB, but Not p53, in Skeletal Muscle during Denervation-Induced Plasticity

Immunoprecipitation (IP) of CARM1 was performed in WT TA muscles to assess potential functional interactions of CARM1 with AMPK, FOXO1, TFEB, and p53. These proteins are well-known mediators of muscle phenotype determination and remodeling (Kjøbsted et al., 2018; Hood et al., 2019), while we and others have previously shown that AMPK and FOXO proteins interact with PRMTs in skeletal muscle (Stouth et al., 2018; Liu et al., 2019; Yamagata et al., 2008). Moreover, TFEB and p53 are validated targets of CARM1 in other cell types (Shin et al., 2016; An et al., 2004). Our data show that CARM1 interacted with AMPK, FOXO1, and TFEB in skeletal muscle *in vivo* (Figure 6A). Interestingly, we did not detect an interaction between CARM1 and p53 (Figure 6A). The interaction between CARM1 and AMPK increased by ~1.5-fold ($p < 0.05$) after 3 days in the DEN versus CON limb (Figures 6A and 6B). Relative to the CON limb, the interaction between CARM1 and FOXO1 was significantly greater by ~1.2-fold in the DEN TA muscle after 3 days, whereas the interaction between CARM1 and TFEB decreased by ~43% ($p < 0.05$) in the DEN limb following 7 days.

CARM1 Methylates AMPK in Muscle *In Vivo*

We were particularly interested in determining whether CARM1 could influence the methylation of AMPK during neurogenic muscle disuse. IP of AMPK was carried out in WT and mKO TA muscles, followed by immunoblotting (IB) for ADMA-5^{CARM1} and ADMA^{GAR}. A significant interaction between genotype and denervation for IP of AMPK and IB of ADMA-5^{CARM1} was observed after 3 days of disuse (Figures 6C and 6D). Specifically, in TA muscles with IP of AMPK, denervation induced a ~1.9-fold increase ($p < 0.05$) in ADMA-5^{CARM1} content relative to the CON limb in WT animals, whereas no significant changes were observed in the absence of CARM1. Following IP of AMPK, ADMA^{GAR} content was similar between CON and DEN limbs in the TA muscle of WT and mKO animals after 3 and 7 days (Figures 6C–6E).

CARM1 Regulates AMPK Signaling

Finally, we sought to determine whether CARM1 is required for AMPK activation and downstream signaling in skeletal muscle. As such, we employed the systemic pan-AMPK activator MK-8722 (Myers et al., 2017) to assess pharmacological activation of AMPK and AMPK-mediated, site-specific phosphorylation of ACC in mKO animals. WT and mKO animals were treated with either vehicle (Veh) or MK-8722 by oral gavage. At 3 h post-dose, we observed a main effect ($p < 0.05$) of MK-8722 on P-AMPK^{Thr172} content in both WT and mKO TA muscles (Figures 7A and 7B). For instance, relative to WT Veh and mKO Veh, P-AMPK^{Thr172} content in WT and mKO animals was significantly greater by ~2-fold after MK-8722 administration. Neither genotype nor MK-8722 had an effect on total AMPK content. We also detected a main effect ($p < 0.05$) of MK-8722 on AMPK activation status for both genotypes. The phosphorylation of ACC^{Ser79} exhibited a strong trend ($p = 0.10$) toward an interaction between genotype and MK-8722 in the TA muscle (Figures 7A and 7C). We also observed a main effect ($p < 0.05$) of genotype on P-ACC^{Ser79}. MK-8722 and genotype did not have an effect on total ACC content. An interaction ($p < 0.05$) between genotype and MK-8722 for

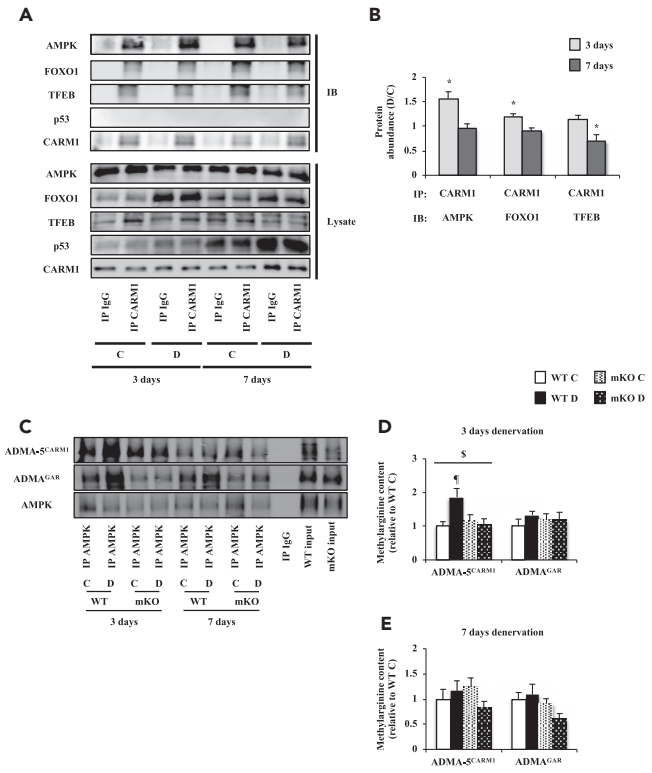

Figure 6. Protein Interactions in Denervated Skeletal Muscle

(A) Representative immunoprecipitation (IP) images of CARM1 or immunoglobulin G (IgG) with subsequent immunoblotting (IB) for AMPK, FOXO1, TFEB, p53, and CARM1 in D and C TA muscles following 3 and 7 days of denervation in WT mice. Western blots of whole muscle lysates (Lysate) for AMPK, FOXO1, TFEB, p53, and CARM1 are also shown.

(B) Graphical summary of CARM1 interactions with AMPK, FOXO1, and TFEB following 3 and 7 days of neurogenic muscle disuse. Data are expressed as protein abundance ratio in D versus C (n = 7–10). Data are means ± SEM. Student's t test; *p < 0.05 D versus C.

(C) Typical images of IP of AMPK with IB for ADMA-5^{CARM1}, ADMA^{GAR}, and AMPK in TA muscles from the C and D hindlimbs of WT and mKO mice following 3 and 7 days of denervation. Representative lanes of IP of IgG, as well as WT and mKO inputs (i.e., whole muscle lysate precleared with IgG) are also shown. Graphical summaries of methylated AMPK levels in WT and mKO animals after 3 (D) and 7 (E) days of denervation. Data are expressed as methylated protein content relative to WT C (n = 5–8). Data are means ± SEM. Two-way ANOVA; $p < 0.05 interaction effect of genotype and denervation; ¶p < 0.05 versus WT C.

ACC activation status emerged 3 h after the dose. Specifically, relative to WT mice treated with Veh, MK-8722 induced a ~1.9-fold increase ($p < 0.05$) in ACC activation status in WT animals, whereas no significant changes were observed in the absence of CARM1. A main effect ($p < 0.05$) of genotype on ACC activation status was also apparent. Furthermore, we detected a significant main effect of genotype on total TBC1 domain family member 1 (TBC1D1), TBC1D1 activation status, phosphorylation of FOXO3^{Ser588}, as well as FOXO3 activation status (Figures 7A, 7D, and 7E).

We further investigated the impact of CARM1 deletion on AMPK signaling by probing a panel of genes downstream of AMPK. In particular, we assessed PGC-1α, p53, Tfam, p62, MuRF1, and MAFbx transcript levels in the EDL because these genes are influenced by AMPK activity (Ljubicic et al., 2014; Ha et al., 2017; Kjøbsted et al., 2018). We detected a main effect ($p < 0.05$) of MK-8722 on PGC-1α and MuRF1 transcript levels in the EDL muscle after treatment (Figure 7F). PGC-1α and MuRF1 exhibited a trend toward an interaction between genotype and MK-8722 after 3 h of the dose ($p = 0.13$ and $p = 0.10$, respectively). A main effect ($p < 0.05$) of genotype on p53 and MAFbx transcript levels was also observed in the EDL muscles. Genotype and MK-8722 did not have an effect on Tfam and p62 mRNA content.

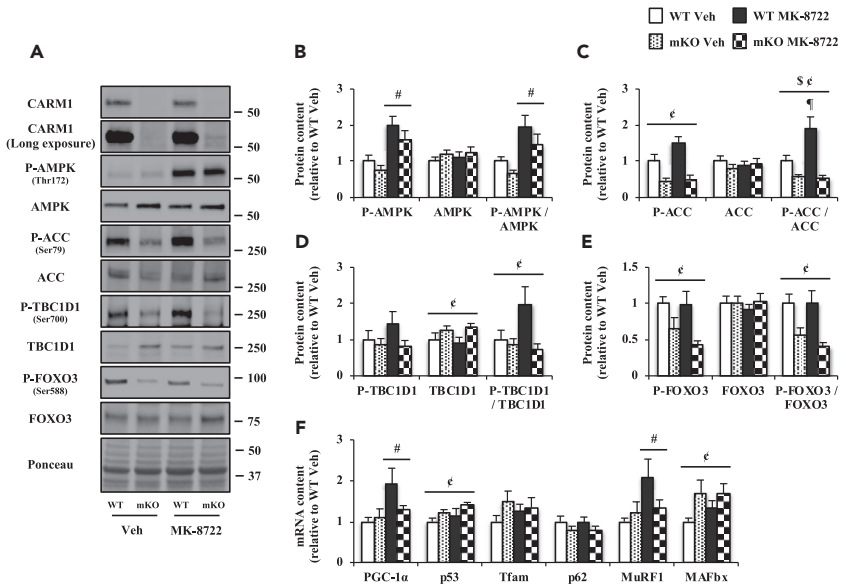

Figure 7. CARM1 Regulates AMPK Signaling

(A) Representative western blots of CARM1 (normal and long exposure), P-AMPK^{Thr172}, total AMPK, P-ACC^{Ser79}, total ACC, phosphorylated TBC1 domain family member 1 (P-TBC1D1)^{Ser700}, total TBC1D1, P-FOXO3^{Ser588}, and FOXO3 protein content in WT and mKO TA muscles after an acute dose (3 h) of vehicle (Veh) or MK-8722, accompanied by a typical Ponceau stain. Molecular weights (kDa) are shown on the right of blots.

(B–E) Graphical summaries of P-AMPK^{Thr172}, AMPK, AMPK activation status, P-ACC^{Ser79}, ACC, ACC activation status, P-TBC1D1^{Ser700}, TBC1D1, TBC1D1 activation status, P-FOXO3^{Ser588}, FOXO3, and FOXO3 activation status in WT and mKO TA muscles following Veh or MK-8722 administration. Data are expressed as protein content relative to WT Veh (n = 6–9).

(F) PGC-1α, p53, Tfam, p62, MuRF1, and MAFbx mRNA expression in EDL muscles from WT and mKO animals following Veh or MK-8722 treatment. Data are expressed as mRNA content relative to WT Veh (n = 6–8). Data are means ± SEM. Two-way ANOVA; $p < 0.05 interaction effect of genotype and MK-8722; ¢p < 0.05 main effect of genotype; #p < 0.05 main effect of MK-8722; ¶p < 0.05 versus WT Veh.

DISCUSSION

Our results show that CARM1 is required to maintain muscle mass and skeletal muscle-specific deletion of CARM1 impacts AMPK signaling. We also demonstrate that CARM1 interacts with and methylates AMPK in skeletal muscle and that this interaction is increased during the early adaptive response to neurogenic muscle disuse. Consistent with this, CARM1 mKO resulted in attenuated phosphorylation of AMPK and proximate autophagic and atrophic signaling following 3 days of denervation. Moreover, we found that in contrast to muscles from WT mice, MK-8722 evoked AMPK site-specific activation of ACC^{Ser79} and TBC1D1^{Ser700}, as well as the gene expression of downstream AMPK targets PGC-1α and MuRF1 did not change in mKO muscles. Collectively, these genetic, physiologic, and pharmacologic data indicate that CARM1 regulates AMPK signaling in skeletal muscle.

We detected muscle-specific differences in the role of CARM1 in the maintenance of skeletal muscle mass. For instance, muscle mass of the fast, glycolytic TA, as well as EDL myofiber CSA, was lower in mKO versus WT mice, whereas SOL muscle mass was greater in mKO animals. These results align with previous work demonstrating that transient knockdown of CARM1 reduces TA muscle weight (Liu et al., 2019). Autophagy is required to maintain muscle mass (Masiero et al., 2009; Carnio et al., 2014), and loss of CARM1 compromises the autophagic process (Shin et al., 2016; Liu et al., 2019). As AMPK promotes autophagy (Kjøbsted et al., 2018; Bujak et al., 2015), in part through stabilization of CARM1 (Shin et al., 2016), it is reasonable to speculate that knocking out CARM1 in skeletal muscle altered AMPK signaling and dysregulated downstream autophagic processes that contributed to the differential muscle phenotype between WT and mKO animals. The experimental evidence revealed here strongly supports this assertion. First, we show that under basal conditions in skeletal muscle CARM1 interacts with AMPK. Second, knocking out CARM1 attenuated basal levels of AMPK-mediated ACC^{Ser79} and FOXO3^{Ser588} phosphorylation. Third, CARM1 mKO resulted in elevated protein content of Beclin1, whose expression levels, as well as dual

regulation of autophagy and apoptosis, are controlled by AMPK-mediated phosphorylation (Kim et al., 2013; Song et al., 2014; Zhang et al., 2016). Fourth, we demonstrate that CARM1 interacts with TFEB and FOXO1, master transcriptional regulators of the autophagy and atrophy programs, respectively. CARM1 exerts transcriptional co-activator function on TFEB (Shin et al., 2016) whereas TFEB regulates AMPK signaling in skeletal muscle (Mansueto et al., 2017). Atrophy-related genes that are governed, in part, by FOXO1 (Bodine, 2013; Milan et al., 2015) were upregulated in response to CARM1 deletion. In particular, MAFbx transcript levels were greater in mKO versus WT muscle. RNA sequencing analysis also revealed disparate atrophy-related gene expression profiles between genotypes, such as increased FOXO1 transcript levels in mKO versus WT animals (data not shown). Finally, we observed augmented PGC-1α content in mKO muscle. AMPK modulates the function of PGC-1α (Dial et al., 2018; Kjøbsted et al., 2018), a transcriptional coactivator that elicits lysosomal and autophagosomal biogenesis in skeletal muscle (Takikita et al., 2010; Halling et al., 2016; Erlich et al., 2018). In all, the data indicate that skeletal muscle phenotypic plasticity in mKO mice is due, at least in part, to altered autophagic signaling mediated by the dissociation of CARM1-AMPK complexes.

It was previously demonstrated that CARM1 knockdown attenuated atrophy and the expression of atrogenes following 28 days of neurogenic muscle disuse (Liu et al., 2019). Consistent with this, the present study shows that knocking out CARM1 in muscle mitigated the progression of denervation-induced skeletal muscle atrophy. This may be due to a specific effect of CARM1 deletion, or possibly to mKO muscles already nearing maximal atrophy, or a combination thereof. We postulate that the induction of PGC-1α in mKO animals resulted in increased protection from relatively short-term (i.e., 3 and 7 days) denervation-induced atrophy, but was unable to preserve muscle mass against a lifetime (i.e., 12 weeks old) of potentially dysregulated atrophy and autophagy signaling and gene expression. Furthermore, our data strongly suggest that CARM1 regulates neurogenic disuse-evoked muscle wasting by way of AMPK. AMPK is activated during various conditions of disuse, whereas AMPK deficiency protects muscle from atrophy (Kjøbsted et al., 2018). AMPK promotes autophagic and proteasomal-mediated protein degradation by phosphorylating ULK1^{Ser555} and FOXO3^{Ser588}, respectively (Kjøbsted et al., 2018). Here, we observed reduced AMPK activation, attenuated downstream stimulatory phosphorylation of ULK^{Ser555} and FOXO3^{Ser588}, as well as mitigated expression levels of FOXO-mediated atrogenes MuRF1 and MAFbx in mKO mice compared with their WT littermates after 3 days of neurogenic muscle disuse. These data suggest that the absence of CARM1 alters AMPK-mediated atrophic signaling during the early adaptive response to denervation. Consistent with this, our IP experiments in WT animals revealed an increased interaction between CARM1 and FOXO1 following 3 days of disuse. As CARM1 modulates the expression of atrophy-related genes by activating FOXO3 via its asymmetric arginine dimethylation (Liu et al., 2019), it is reasonable to posit that CARM1 exerts a similar function on FOXO1 based on the (1) presence of proline-rich CARM1 methylation motifs on FOXO1 at Arg19 and Arg29 (Lee and Bedford, 2002; Gayatri et al., 2016; Cheng et al., 2018) as well as (2) comparable functions between FOXO1 and FOXO3 (Bodine, 2013). Blunted p53 mRNA and protein responses in mKO mice after 3 and 7 days of denervation, respectively, further support the role of a CARM1-AMPK signaling axis in governing muscle phenotype. Indeed, AMPK activation upregulates p53 levels (Imamura et al., 2001) and AMPK-mediated phosphorylation of p53^{Ser15} stabilizes the protein (Jones et al., 2005). Interestingly, we were unable to detect CARM1-p53 interactions in skeletal muscle despite previously observed complexes comprising these molecules (An et al., 2004; O'Brien et al., 2010).

Skeletal muscle-specific PRMT1 deletion results in elevated CARM1 expression (Choi et al., 2019). In contrast, we demonstrate that knocking out CARM1 in skeletal muscle does not influence PRMT1 or PRMT5 content, or their corresponding outputs of global methyltransferase activities ADMA^{GAR} and SDMA, respectively. We also probed methyl-GAR and methyl-CARM1 motifs to assess myocellular ADMA levels, as well as the asymmetric marking of dimethylarginines preferentially performed by CARM1, respectively (Guo et al., 2014; Cheng et al., 2018). We did not observe altered deposition of the ADMA^{GAR} mark in mKO animals, likely because CARM1 does not methylate this motif and because there was no compensatory alteration in PRMT1 activity. Conversely, and as expected, ADMA-5^{CARM1} levels were significantly lower in mKO versus WT mice. We reason that ADMA-5^{CARM1} was not completely ablated in mKO mice due to (1) residual CARM1 activity in cells other than myocytes that typically reside in the muscle and (2) off-target ADMA activity by PRMT1 (Cheng et al., 2018). Denervation elicited increased CARM1 protein and ADMA-5^{CARM1} levels in WT, but not mKO animals, suggesting that CARM1 content and its specific

methyltransferase activity are closely linked during disuse-evoked muscle remodeling. We further demonstrate that denervation-induced methylation of AMPK specifically by CARM1 occurred coincident with increased CARM1-AMPK binding and AMPK activation. Indeed, deposition of ADMA-5^{CARM1} on AMPK was elevated in DEN versus CON muscles following 3 days of disuse in WT animals. In contrast, the ADMA-5^{CARM1} mark on AMPK did not differ between CON and DEN limbs in mKO animals, whereas AMPK ADMA^{GAR} levels remained unchanged in response to denervation in both genotypes. Together these data strongly indicate that CARM1 was solely responsible for the augmented arginine methylation of AMPK during denervation. Our results reveal a CARM1-AMPK mechanism in the skeletal muscle atrophy program during the early adaptive response to neurogenic disuse. A rational hypothesis is that the methyltransferase marks the AMPKα1 subunit at a partially conserved CARM1 ADMA site located at the Arg538 proline-rich motif (Lee and Bedford, 2002; Gayatri et al., 2016; Cheng et al., 2018). Notably, the α-subunit is required for AMPK catalytic activity, and AMPKα1 indirectly promotes muscle atrophy by antagonizing anabolic signaling (Phillips et al., 2009; Kjøbsted et al., 2018).

MK-8722 is a potent pharmacological activator of all 12 AMPK isoforms (Myers et al., 2017; Muise et al., 2019). The compound directly binds to the allosteric drug and metabolite site located at the interface between the α-subunit kinase domain and the carbohydrate-binding module in the β-subunit, which is thought to protect Thr172 from dephosphorylation (Steinberg and Carling, 2019). Our data indicate that whereas CARM1 is dispensable for MK-8722-mediated phosphorylation of AMPK, MK-8722-induced activation status of ACC^{Ser79} and TBC1D1^{Ser700} were abolished in the absence of CARM1. Indeed, AMPK-regulated genes, such as PGC-1α and MuRF1 tended to be blunted in mKO animals after MK-8722 administration, further supporting the assertion that CARM1 affects AMPK signaling. It is interesting to note that, contrary to 3 days of denervation, acute 3-h administration of MK-8722 evoked increased AMPK^{Thr172} phosphorylation in muscles from both WT and mKO animals. These data highlight distinct influences of CARM1 on AMPK during physiological versus pharmacological activation of the kinase. We suspect that a regulatory loop between CARM1 and AMPK exists, as in some conditions CARM1 functions downstream of AMPK (Shin et al., 2016) and the methyltransferase contains a well-defined AMPK phosphorylation motif at Ser501 (Hardie et al., 2016; Steinberg and Carling, 2019).

In summary, this study reveals a CARM1-AMPK mechanism that impacts the maintenance and remodeling of muscle mass via altered downstream autophagic and atrophic signaling. Given the emerging roles for CARM1 in muscle biology (Stouth et al., 2017; vanLieshout et al., 2019), as well as the established functions for AMPK in maintaining and remodeling skeletal muscle phenotype (Mounier et al., 2015; Dial et al., 2018; Kjøbsted et al., 2018; Steinberg and Carling, 2019), targeting this interplay between CARM1-AMPK may therefore provide therapeutic strategies for myopathies such as disuse atrophy, the sarcopenia of aging, or cancer cachexia.

Limitations of the Study

We note several limitations in this study. First, only male mice were examined, at one age and after fixed periods and mode of muscle atrophy. It is possible that female mice or mice of a different age would have different responses to CARM1 mKO, or that different durations of neurogenic disuse, or different models of atrophy (e.g., fasting, unweighting, advanced aging), would differentially impact CARM1-AMPK signaling. Second, we engineered and utilized CARM1 mKO animals to reveal the role of the methyltransferase in skeletal muscle. An inducible CARM1 mKO model, for example, elicited by tamoxifen treatment (McCarthy et al., 2012), would introduce temporal specificity to the removal of CARM1 in muscle and control for any compensatory or confounding adaptations that may have occurred in the animals across a lifetime without the enzyme. Third, the molecular mechanisms of muscle atrophy in humans do not mirror precisely the events that transpire in murine muscle (Atherton et al., 2016). Future work is needed to test and extend the current findings in skeletal muscle from human participants (vanLieshout et al., 2019). Finally, although we demonstrated that CARM1 methylated AMPK in muscle, further research is needed to confirm specific methylation site(s) on the kinase. Other CARM1 targets, as well as the arginine methylome in skeletal muscle, also require identification.

Resource Availability

Lead Contact

Further information and requests for resources and reagents should be directed to and will be fulfilled by the Lead Contact, Dr. Vladimir Ljubicic (ljubicic@mcmaster.ca).

Materials Availability

This study did not generate any unique reagents.

Data and Code Availability

This study did not generate datasets/code.

METHODS

All methods can be found in the accompanying Transparent Methods supplemental file.

SUPPLEMENTAL INFORMATION

Supplemental Information can be found online at https://doi.org/10.1016/j.isci.2020.101755.

ACKNOWLEDGMENTS

We thank Dr. Mark Bedford (MD Anderson Cancer Center, University of Texas) and Dr. Anne Brunet (Department of Genetics, Stanford University School of Medicine) for the gifts of CARM1 floxed mice and the ADMA-5^{CARM1} reagent, as well as the P-FOXO3^{Ser588} antibody, respectively. We also thank Dr. Lawrence Kazak (McGill University, Canada) for assistance with genotyping. We are grateful to members of the Integrative Neuromuscular Biology Laboratory and to colleagues in the Exercise Metabolism Research Group at McMaster University for helpful advice and discussion. This work was funded by the Natural Sciences and Engineering Research Council of Canada (NSERC), the Canada Research Chairs program, and the Ontario Ministry of Economic Development, Job Creation and Trade (MEDJCT). D.W.S., T.L.v., and S.Y.N. are NSERC postgraduate scholars. E.K.W. is an Interdisciplinary Fellow of the Canadian Frailty Network. V.L. is the Canada Research Chair (Tier 2) in Neuromuscular Plasticity in Health and Disease, and is a MEDJCT Early Researcher.

AUTHOR CONTRIBUTIONS

D.W.S. and V.L. conceived and designed the study; D.W.S. and T.L.v. generated and maintained CARM1 mKO mice; D.W.S. performed denervation surgeries, quantitative real-time RT-PCRs, western blot and immunoprecipitation experiments; D.W.S. and Z.M. conducted H&E staining analyses; E.K.W. and A.M. assisted with western blot procedures; D.W.S. and A.M. executed SDH staining technique; S.Y.N. performed MK-8722 experiments; all authors participated in data analysis and interpretation of results; D.W.S. and V.L. drafted and edited the manuscript.

DECLARATION OF INTERESTS

The authors declare no competing interests.

Received: May 15, 2020
Revised: September 28, 2020
Accepted: October 28, 2020
Published: November 20, 2020

REFERENCES

An, W., Kim, J., and Roeder, R.G. (2004). Ordered cooperative functions of PRMT1, p300, and CARM1 in transcriptional activation by p53. Cell *117*, 735–748.

Atherton, P.J., Greenhaff, P.L., Phillips, S.M., Bodine, S.C., Adams, C.M., and Lang, C.H. (2016). Control of skeletal muscle atrophy in response to disuse: clinical/preclinical contentions and fallacies of evidence. Am. J. Physiol. Endocrinol. Metab. *311*, E594–E604.

Bao, J., Rousseaux, S., Shen, J., Lin, K., Lu, Y., and Bedford, M.T. (2018). The arginine methyltransferase CARM1 represses p300●ACT●CREMτ activity and is required for spermiogenesis. Nucleic Acids Res. *46*, 4327–4343.

Bedford, M.T., and Clarke, S.G. (2009). Protein arginine methylation in mammals: who, what, and why. Mol. Cell *33*, 1–13.

Bodine, S.C. (2013). Disuse-induced muscle wasting. Int. J. Biochem. Cell Biol. *45*, 2200–2208.

Bujak, A.L., Crane, J.D., Lally, J.S., Ford, R.J., Kang, S.J., Rebalka, I.A., Green, A.E., Kemp, B.E., Hawke, T.J., Schertzer, J.D., and Steinberg, G.R. (2015). AMPK activation of muscle autophagy prevents fasting-induced hypoglycemia and myopathy during aging. Cell Metab. *21*, 883–890.

Carnio, S., LoVerso, F., Baraibar, M.A., Longa, E., Khan, M.M., Maffei, M., Reischl, M., Canepari, M., Loefler, S., Kern, H., et al. (2014). Autophagy impairment in muscle induces neuromuscular junction degeneration and precocious aging. Cell Rep. *8*, 1509–1521.

Chang, N.C., Sincennes, M.C., Chevalier, F.P., Brun, C.E., Lacaria, M., Segalés, J., Muñoz-Cánoves, P., Ming, H., and Rudnicki, M.A. (2018). The Dystrophin Glycoprotein complex regulates the epigenetic activation of muscle stem cell commitment. Cell Stem Cell *22*, 755–768.e6.

Chen, S.L., Loffler, K.A., Chen, D., Stallcup, M.R., and Muscat, G.E. (2002). The

coactivator-associated arginine methyltransferase is necessary for muscle differentiation: CARM1 coactivates myocyte enhancer factor-2. J. Biol. Chem. *277*, 4324–4333.

Cheng, D., Vemulapalli, V., Lu, Y., Shen, J., Aoyagi, S., Fry, C.J., Yang, Y., Foulds, C.E., Stossi, F., Treviño, L.S., et al. (2018). CARM1 methylates MED12 to regulate its RNA-binding ability. Life Sci. Alliance *1*, e201800117.

Choi, S., Jeong, H.J., Kim, H., Choi, D., Cho, S.C., Seong, J.K., Koo, S.H., and Kang, J.S. (2019). Skeletal muscle-specific Prmt1 deletion causes muscle atrophy via deregulation of the PRMT6-FOXO3 axis. Autophagy *15*, 1069–1081.

Dial, A.G., Ng, S.Y., Manta, A., and Ljubicic, V. (2018). The role of AMPK in neuromuscular biology and disease. Trends Endocrinol. Metab. *29*, 300–312.

Erlich, A.T., Brownlee, D.M., Beyfuss, K., and Hood, D.A. (2018). Exercise induces TFEB expression and activity in skeletal muscle in a PGC-1α-dependent manner. Am. J. Physiol. Cell Physiol. *314*, C62–C72.

Fulton, M.D., Brown, T., and Zheng, Y.G. (2019). The biological Axis of protein arginine methylation and asymmetric dimethylarginine. Int. J. Mol. Sci. *20*, 3322.

Gayatri, S., Cowles, M.W., Vemulapalli, V., Cheng, D., Sun, Z.W., and Bedford, M.T. (2016). Using oriented peptide array libraries to evaluate methylarginine-specific antibodies and arginine methyltransferase substrate motifs. Sci. Rep. *6*, 28718.

Guccione, E., and Richard, S. (2019). The regulation, functions and clinical relevance of arginine methylation. Nat. Rev. Mol. Cell Biol. *20*, 642–657.

Guo, A., Gu, H., Zhou, J., Mulhern, D., Wang, Y., Lee, K.A., Yang, V., Aguiar, M., Kornhauser, J., Jia, X., et al. (2014). Immunoaffinity enrichment and mass spectrometry analysis of protein methylation. Mol. Cell Proteomics *13*, 372–387.

Ha, S., Jeong, S.H., Yi, K., Chung, K.M., Hong, C.J., Kim, S.W., Kim, E.K., and Yu, S.W. (2017). Phosphorylation of p62 by AMP-activated protein kinase mediates autophagic cell death in adult hippocampal neural stem cells. J. Biol. Chem. *292*, 13795–13808.

Halling, J.F., Ringholm, S., Nielsen, M.M., Overby, P., and Pilegaard, H. (2016). PGC-1α promotes exercise-induced autophagy in mouse skeletal muscle. Physiol. Rep. *4*, e12698.

Hardie, D.G., Schaffer, B.E., and Brunet, A. (2016). AMPK: an energy-sensing pathway with multiple inputs and outputs. Trends Cell Biol. *26*, 190–201.

Hood, D.A., Memme, J.M., Oliveira, A.N., and Triolo, M. (2019). Maintenance of skeletal muscle Mitochondria in health, exercise, and aging. Annu. Rev. Physiol. *81*, 19–41.

Imamura, K., Ogura, T., Kishimoto, A., Kaminishi, M., and Esumi, H. (2001). Cell cycle regulation via p53 phosphorylation by a 5′-AMP activated protein kinase activator, 5-aminoimidazole- 4-carboxamide-1-beta-D-ribofuranoside, in a human hepatocellular carcinoma cell line. Biochem. Biophys. Res. Commun. *287*, 562–567.

Jones, R.G., Plas, D.R., Kubek, S., Buzzai, M., Mu, J., Xu, Y., Birnbaum, M.J., and Thompson, C.B. (2005). AMP-activated protein kinase induces a p53-dependent metabolic checkpoint. Mol. Cell *18*, 283–293.

Kawabe, Y., Wang, Y.X., McKinnell, I.W., Bedford, M.T., and Rudnicki, M.A. (2012). Carm1 regulates Pax7 transcriptional activity through MLL1/2 recruitment during asymmetric satellite stem cell divisions. Cell Stem Cell *11*, 333–345.

Kim, D., Lim, S., Park, M., Choi, J., Kim, J., Han, H., Yoon, K., Kim, K., Lim, J., and Park, S. (2014). Ubiquitination-dependent CARM1 degradation facilitates Notch1-mediated podocyte apoptosis in diabetic nephropathy. Cell Signal. *26*, 1774–1782.

Kim, J., Kim, Y.C., Fang, C., Russell, R.C., Kim, J.H., Fan, W., Liu, R., Zhong, Q., and Guan, K.L. (2013). Differential regulation of distinct Vps34 complexes by AMPK in nutrient stress and autophagy. Cell *152*, 290–303.

Kjøbsted, R., Hingst, J.R., Fentz, J., Foretz, M., Sanz, M.N., Pehmøller, C., Shum, M., Marette, A., Mounier, R., Treebak, J.T., et al. (2018). AMPK in skeletal muscle function and metabolism. FASEB J. *32*, 1741–1777.

Larsen, S.C., Sylvestersen, K.B., Mund, A., Lyon, D., Mullari, M., Madsen, M.V., Daniel, J.A., Jensen, L.J., and Nielsen, M.L. (2016). Proteome-wide analysis of arginine monomethylation reveals widespread occurrence in human cells. Sci. Signal. *9*, rs9.

Lee, J., and Bedford, M.T. (2002). PABP1 identified as an arginine methyltransferase substrate using high-density protein arrays. EMBO Rep. *3*, 268–273.

Liu, Y., Li, J., Shang, Y., Guo, Y., and Li, Z. (2019). CARM1 contributes to skeletal muscle wasting by mediating FoxO3 activity and promoting myofiber autophagy. Exp. Cell Res. *374*, 198–209.

Ljubicic, V., Burt, M., and Jasmin, B.J. (2014). The therapeutic potential of skeletal muscle plasticity in Duchenne muscular dystrophy: phenotypic modifiers as pharmacologic targets. FASEB J. *28*, 548–568.

Ljubicic, V., Khogali, S., Renaud, J.M., and Jasmin, B.J. (2012). Chronic AMPK stimulation attenuates adaptive signaling in dystrophic skeletal muscle. Am. J. Physiol. Cell Physiol. *302*, C110–C121.

Mansueto, G., Armani, A., Viscomi, C., D'Orsi, L., De Cegli, R., Polishchuk, E.V., Lamperti, C., Di Meo, I., Romanello, V., Marchet, S., et al. (2017). Transcription factor EB controls metabolic flexibility during exercise. Cell Metab. *25*, 182–196.

Masiero, E., Agatea, L., Mammucari, C., Blaauw, B., Loro, E., Komatsu, M., Metzger, D., Reggiani, C., Schiaffino, S., and Sandri, M. (2009). Autophagy is required to maintain muscle mass. Cell Metab. *10*, 507–515.

McCarthy, J.J., Srikuea, R., Kirby, T.J., Peterson, C.A., and Esser, K.A. (2012). Inducible Cre transgenic mouse strain for skeletal muscle-specific gene targeting. Skelet Muscle *2*, 8.

Milan, G., Romanello, V., Pescatore, F., Armani, A., Paik, J.H., Frasson, L., Seydel, A., Zhao, J., Abraham, R., Goldberg, A.L., et al. (2015). Regulation of autophagy and the ubiquitin-proteasome system by the FoxO transcriptional network during muscle atrophy. Nat. Commun. *6*, 6670.

Mounier, R., Théret, M., Lantier, L., Foretz, M., and Viollet, B. (2015). Expanding roles for AMPK in skeletal muscle plasticity. Trends Endocrinol. Metab. *26*, 275–286.

Muise, E.S., Guan, H.P., Liu, J., Nawrocki, A.R., Yang, X., Wang, C., Rodríguez, C.G., Zhou, D., Gorski, J.N., Kurtz, M.M., et al. (2019). Pharmacological AMPK activation induces transcriptional responses congruent to exercise in skeletal and cardiac muscle, adipose tissues and liver. PLoS One *14*, e0211568.

Myers, R.W., Guan, H.P., Ehrhart, J., Petrov, A., Prahalada, S., Tozzo, E., Yang, X., Kurtz, M.M., Trujillo, M., Gonzalez Trotter, D., et al. (2017). Systemic pan-AMPK activator MK-8722 improves glucose homeostasis but induces cardiac hypertrophy. Science *357*, 507–511.

O'Brien, K.B., Alberich-Jordà, M., Yadav, N., Kocher, O., Diruscio, A., Ebralidze, A., Levantini, E., Sng, N.J., Bhasin, M., Caron, T., et al. (2010). CARM1 is required for proper control of proliferation and differentiation of pulmonary epithelial cells. Development *137*, 2147–2156.

Phillips, S.M., Glover, E.I., and Rennie, M.J. (2009). Alterations of protein turnover underlying disuse atrophy in human skeletal muscle. J. Appl. Physiol. *107*, 645–654.

Sandri, M. (2013). Protein breakdown in muscle wasting: role of autophagy-lysosome and ubiquitin-proteasome. Int. J. Biochem. Cell Biol. *45*, 2121–2129.

Shen, N.Y., Ng, S.Y., Toepp, S.L., and Ljubicic, V. (2018). Protein arginine methyltransferase expression and activity during myogenesis. Biosci. Rep. *38*, 1.

Shin, H.J., Kim, H., Oh, S., Lee, J.G., Kee, M., Ko, H.J., Kweon, M.N., Won, K.J., and Baek, S.H. (2016). AMPK-SKP2-CARM1 signalling cascade in transcriptional regulation of autophagy. Nature *534*, 553–557.

Song, X., Kim, S.Y., Zhang, L., Tang, D., Bartlett, D.L., Kwon, Y.T., and Lee, Y.J. (2014). Role of AMP-activated protein kinase in cross-talk between apoptosis and autophagy in human colon cancer. Cell Death Dis. *5*, e1504.

Steinberg, G.R., and Carling, D. (2019). AMP-activated protein kinase: the current landscape for drug development. Nat. Rev. Drug Discov. *18*, 527–551.

Stouth, D.W., Manta, A., and Ljubicic, V. (2018). Protein arginine methyltransferase expression, localization, and activity during disuse-induced skeletal muscle plasticity. Am. J. Physiol. Cell Physiol. *314*, C177–C190.

Stouth, D.W., vanLieshout, T.L., Shen, N.Y., and Ljubicic, V. (2017). Regulation of skeletal muscle plasticity by protein arginine methyltransferases and their potential roles in neuromuscular disorders. Front Physiol. *8*, 870.

Takikita, S., Schreiner, C., Baum, R., Xie, T., Ralston, E., Plotz, P.H., and Raben, N. (2010). Fiber type conversion by PGC-1α activates lysosomal and autophagosomal biogenesis in both unaffected and Pompe skeletal muscle. PLoS One *5*, e15239.

Vainshtein, A., Grumati, P., Sandri, M., and Bonaldo, P. (2014). Skeletal muscle, autophagy, and physical activity: the ménage à trois of metabolic regulation in health and disease. J. Mol. Med. (Berl) *92*, 127–137.

vanLieshout, T.L., and Ljubicic, V. (2019). The emergence of protein arginine methyltransferases in skeletal muscle and metabolic disease. Am. J. Physiol. Endocrinol. Metab. *317*, E1070–E1080.

vanLieshout, T.L., Bonafiglia, J.T., Gurd, B.J., and Ljubicic, V. (2019). Protein arginine methyltransferase biology in humans during acute and chronic skeletal muscle plasticity. J. Appl. Physiol. *127*, 867–880.

Vanlieshout, T.L., Stouth, D.W., Tajik, T., and Ljubicic, V. (2018). Exercise-induced protein arginine methyltransferase expression in skeletal muscle. Med. Sci. Sports Exerc. *50*, 447–457.

Wang, S.C., Dowhan, D.H., Eriksson, N.A., and Muscat, G.E. (2012). CARM1/PRMT4 is necessary for the glycogen gene expression programme in skeletal muscle cells. Biochem. J. *444*, 323–331.

Yadav, N., Lee, J., Kim, J., Shen, J., Hu, M.C., Aldaz, C.M., and Bedford, M.T. (2003). Specific protein methylation defects and gene expression perturbations in coactivator associated arginine methyltransferase 1-deficient mice. Proc. Natl. Acad. Sci. U S A *100*, 6464–6468.

Yamagata, K., Daitoku, H., Takahashi, Y., Namiki, K., Hisatake, K., Kako, K., Mukai, H., Kasuya, Y., and Fukamizu, A. (2008). Arginine methylation of FOXO transcription factors inhibits their phosphorylation by Akt. Mol. Cell *32*, 221–231.

Yang, Y., and Bedford, M.T. (2013). Protein arginine methyltransferases and cancer. Nat. Rev. Cancer *13*, 37–50.

Zhang, D., Wang, W., Sun, X., Xu, D., Wang, C., Zhang, Q., Wang, H., Luo, W., Chen, Y., Chen, H., and Liu, Z. (2016). AMPK regulates autophagy by phosphorylating BECN1 at threonine 388. Autophagy *12*, 1447–1459.

iScience, Volume *23*

Supplemental Information

CARM1 Regulates AMPK Signaling in Skeletal Muscle

Derek W. Stouth, Tiffany L. vanLieshout, Sean Y. Ng, Erin K. Webb, Alexander Manta, Zachary Moll, and Vladimir Ljubicic

Supplemental Information

Transparent Methods

Animals and genotyping

We utilized the Cre/loxP system to generate skeletal muscle-specific CARM1 knockout (mKO) mice. CARM1 floxed animals (Yadav *et al*., 2003; Bao *et al.,* 2018) were a kind gift from Dr. Mark Bedford (The University of Texas MD Anderson Cancer Centre, Smithville, TX, USA). Floxed CARM1 mice (wild type; WT) were generated as described previously in the mixed C57BL6J/129 background. Human α-skeletal actin (HSA)-Cre mice were obtained from Jackson Laboratories (Bar Harbor, ME, USA). HSA-Cre activity is restricted to skeletal muscle (McCarthy *et al.,* 2012). WT and mKO mice were identified via genotyping, using conventional reverse transcription-polymerase chain reaction (RT-PCR) and gel electrophoresis techniques of DNA extracted from tail tissue. The following primers were used to confirm that WT and mKO mice contained a LoxP site for CARM1 between exon 2 and 3: forward (F)-AGTTGGTGACCCTTGTGTCC, reverse (R)-AGCTGCCAGGACCTCTGATA. The following primers were used to distinguish mKO mice that express Cre recombinase: F-GCGGTCTGGCAGTAAAAACTATC, R-GTGAAACAGCATTGCTGTCACTT. For these studies, 12-week-old WT and mKO mice (~25 g body mass; male) were housed in an environmentally controlled room (23 °C, 12-hour light/12-hour dark cycle) and provided food and water ad libitum. Animals were housed at the Central Animal Facility at McMaster University and all protocols were approved by the University Animal Research Ethics Board operating under the auspices of the Canadian Council for Animal Care.

Animal surgery

To elicit denervation-induced skeletal muscle atrophy, WT and mKO mice underwent unilateral sectioning of the sciatic nerve as described previously (Stouth et al. 2018). This model of acquired neurogenic muscle disuse evokes a rapid, robust, and reproducible remodeling of skeletal muscle, while also allowing for the use of the contralateral, innervated limb to serve as an intra-animal control (Sacheck et al. 2007). Briefly, animals were anesthetized by inhalation of isoflurane (Fresenius Kabi, Bad Homburg, HE, Germany) before surgery and received a 2 mg/kg subcutaneous injection of anafen (Boehringer Ingelheim (Canada) Ltd., Burlington, ON, Canada) for post-operative analgesia. A 1-2 cm skin incision was made in the posterior thigh musculature and blunt dissection was employed to expose the sciatic nerve. Unilateral denervation of the lower limb was induced by excising a ~0.5 cm section of the sciatic nerve in the right hind limb. The overlying musculature was sutured with silk (Ethicon Inc., Somerville, NJ, USA), and the skin was secured using veterinary staples (Mikron Precision Inc., Gardena, CA, USA). WT and mKO mice were subjected to 3 and 7 days of denervation (n = 17-20/ group) followed by euthanasia via cervical dislocation. At each experimental time point, the tibialis anterior (TA), extensor digitorum longus (EDL), soleus (SOL), and gastrocnemius (GAST) muscles from both hind limbs were rapidly excised, weighed, frozen in liquid nitrogen or mounted in optimum cutting temperature compound (Thermo Fisher Scientific Life Sciences, Waltham, MA, USA) then frozen in isopentane cooled with liquid

nitrogen. All muscles were then stored at -80 °C for biochemical analyses. Liver, brain, and heart tissues were also harvested from a small cohort of WT and mKO mice for subsequent analysis of tissue-specific CARM1 expression.

Pharmacological activation of AMPK

A separate cohort of age- and sex-matched WT and mKO animals were treated with vehicle [0.25% (w/v) methylcellulose, 5% (v/v) Polysorbate 80, and 0.02% (w/v) sodium lauryl sulfate in deionized water; Veh] or the next-generation AMPK activator MK-8722 (5 mpk) via oral gavage (n = 6-9/ group), as described previously (Myers et al., 2017). Animals were euthanized via cervical dislocation 3 hours after administration, a time point that corresponds to significantly augmented AMPK site-specific phosphorylation of acetyl–coenzyme A carboxylase (ACC) in skeletal muscle (Myers et al., 2017). The TA and EDL muscles were snap frozen in liquid nitrogen. All tissues were then stored at -80 °C for subsequent biochemical analyses.

Histological analysis

EDL and SOL muscle cross-sections were stained with hematoxylin and eosin (H&E) to assess cross-sectional area (CSA) of individual muscle fibers as described previously (Manta et al. 2019). Briefly, EDL and SOL muscles were first transversely sectioned at 5 μm using a cryostat set at -20°C (Thermo Fisher Scientific Life Sciences, Waltham, MA, USA). Muscle cross-sections were later stained with hematoxylin (Sigma-Aldrich, St. Louis, MO, USA) and eosin (Bioshop Canada Inc., Burlington, ON, Canada), dehydrated with successive 70%, 95%, and 100% ethanol exposures, further dried with xylene (Sigma-Aldrich, St. Louis, MO, USA) and mounted with Permount (Thermo Fisher Scientific Life Sciences, Waltham, MA, USA). H&E-stained muscle sections were imaged using light microscopy at 20x magnification with Nikon Elements Microscopic Imaging Software (Nikon Instruments Inc, Melville, NY, USA). The CSA of 150 myofibers across three individual regions of interest per muscle were measured (NIS-Elements). The investigators performing the image analyses were blinded to all samples (i.e., genotype, treatment, muscle).

EDL muscles were cryosectioned into 8 μm sections and stained for succinate dehydrogenase (SDH) activity as described previously (Thomas et al., 2014). Muscle sections were incubated in a buffer consisting of 0.2 M sodium succinate, 0.2 M phosphate buffer, pH 7.4, and nitro blue tetrazolium (Sigma-Aldrich, St. Louis, MO, USA) at 37°C for one hour. Following the incubation period, muscles were rinsed with distilled water, exposed to 30%, 60%, 90% acetone, and mounted with Permount (Thermo Fisher Scientific Life Sciences, Waltham, MA, USA). Photos of muscle sections were then taken using light microscopy at 20x magnification with Nikon Elements Microscopic Imaging Software (Nikon Instruments Inc, Melville, NY, USA).

RNA isolation and quantitative real-time (q) RT-PCR

Total RNA was isolated from the EDL and SOL muscles as described previously (Stouth et al. 2018). All samples were homogenized in 1 mL of Trizol reagent (Invitrogen, Carlsbad, CA, USA) using stainless steel lysing beads and TissueLyser (Qiagen, Hilden, NRW, Germany) at a frequency of 30 Hz for 5 minutes. Homogenized

samples were then mixed with 200 µL of chloroform (Thermo Fisher Scientific, Waltham, MA, USA), agitated vigorously for 15 seconds and centrifuged at 12,000 x g for 10 minutes. The upper aqueous (RNA) phase was purified using the Total RNA Omega Bio-Tek kit (VWR International, Radnor, PA, USA) as per the instructions provided by the manufacturer. RNA concentration and purity were determined using the NanoDrop 1000 Spectrophotometer (Thermo Fisher Scientific Life Sciences,Waltham, MA, USA). RNA samples were then reverse-transcribed into cDNA using a high-capacity cDNA reverse transcription kit (Thermo Fisher Scientific Life Sciences,Waltham, MA, USA) according to the manufacturer instructions. All individual qRT-PCRs were run in duplicate 6 µL reactions containing GoTaq qPCR Master Mix (Promega, Madison, WI, USA). Data were analyzed using the comparative C_T method (Schmittgen et al. 2008). TATA box-binding protein (TBP) was used as a control housekeeping gene for all experiments, as the C_T values for this gene did not change between non-denervated and denervated muscles within, as well as between, time points (data not shown). This control C_T value was subtracted from the C_T value of the gene of interest [$\Delta C_T = C_{T\ (target\ gene)} - C_{T\ (endogenous\ control)}$]. For our denervation experiment, the mean ΔC_T value from the contralateral, non-denervated control (CON) WT muscle was then subtracted from the ΔC_T values of the denervated (DEN) WT muscle [$\Delta\Delta C_T = \Delta C_{T\ (WT\ DEN)} - C_{T\ (WT\ CON)}$]. This calculation was then repeated for CON and DEN mKO limbs. For the MK-8722 pharmacological intervention, the mean ΔC_T value for the WT Veh group was subtracted from the ΔC_T values of the mKO Veh, WT MK-8722, and mKO MK-8722 treated animals. Results are reported as fold changes using the $\Delta\Delta C_T$ method, calculated as $2^{-\Delta\Delta CT}$.

The following primers were used in our study: CARM1 F-CAACAGCGTCCTCATCCAGT, R-GTCCGCTCACTGAACACAGA; silent mating type information regulator 2 homologue 1 (SIRT1) F-GGAACCTTTGCCTCATCTACA, R-CACCTAGCCTATGACACAACTC; peroxisome proliferator-activated receptor-γ coactivator-1α (PGC-1α) F-AGCCGTGACCAGTGACAACGAG, R-GCTGCATGGTTCTGAGTGCTAAG; tumor-suppressor protein p53 F-CCGACCTATCCTTACCATCATC, R-TTCTTCTGTACGGCGGTCTC; mitochondrial transcription factor A (Tfam) F-TAGGCACCGTATTGCGTGAG, R- GTGCTTTTAGCACGCTCCAC; nuclear factor erythroid 2-related factor 2 (Nrf2) F-TTCTTTCAGCAGCATCCTCTCCAC, R-ACAGCCTTCAATAGTCCCGTCCAG; p62 F-CCCAGTGTCTTGGCATTCTT, R-AGGGAAAGCAGAGGAAGCTC; Beclin1 F-AGGCTGAGGCGGAGAGATT, R- TCCACACTCTTGAGTTCGTCAT; transcription factor EB (TFEB) F-AAGGTTCGGGAGTATCTGTCTG, R-GGGTTGGAGCTGATATGTAGCA; Gabarapl F-CATCGTGGAGAAGGCTCCTA, R-ATACAGCTGGCCCATGGTAG; Cathepsin L F-GTGGACTGTTCTCACGCTCAAG, R-TCCGTCCTTCGCTTCATAGG, lysosomal-associated membrane protein 2 (Lamp2) F-GCTGAACAACAGCCAAATTA, R-CTGAGCCATTAGCCAAATACAT, BCL2 and adenovirus E1B 19-kDa-interacting protein 3 (Bnip3) F-TTCCACTAGCACCTTCTGATGA, R-GAACACCGCATTTACAGAACAA, muscle RING finger 1 (MuRF1) F-CACGTGTGAGGTGCCTACTT, R-

CACCAGCATGGAGATGCAGT, muscle atrophy F-box (MAFbx) F-TGAGCGACCTCAGCAGTTAC, R-ATGGCGCTCCTTCGTACTTC; TBP F-CTGCCACACCAGCTTCTGA, R-TGCAGCAAATCGCTTGGG.

Tissue extracts and Western blotting

Samples were processed as described previously (Stouth et al. 2018). Briefly, frozen TA muscle, heart, liver, and brain were ground to a powder using a porcelain mortar and pestle on liquid nitrogen. Samples were suspended in RIPA buffer (Sigma-Aldrich, St. Louis, MO, USA), supplemented with cOmplete Mini Protease Inhibitor Cocktail (Sigma-Aldrich, St. Louis, MO, USA) and PhosSTOP Phosphatase Inhibitor Cocktail (Sigma-Aldrich, St. Louis, MO, USA). All samples were further homogenized using stainless steel lysing beads and TissueLyser (Qiagen, Hilden, NRW, Germany) at a frequency of 30 Hz for 5 minutes. The lysates were then mixed by end-over end inversion for 60 minutes at 4 °C followed by centrifugation at 14,000 x g for 10 minutes. The supernatants were snap-frozen in liquid nitrogen, and stored at -80 °C for further analysis. The protein concentrations of the supernates were determined using the BCA protein assay (Thermo Fisher Scientific Life Sciences,Waltham, MA, USA). Proteins extracted were resolved on 10-12.5% SDS-PAGE gels or 4-15% precast gradient gels (Bio-Rad Laboratories, Inc., Hercules, CA, USA) and subsequently transferred onto nitrocellulose membranes. After transfer, membranes were stained with Ponceau S solution (Sigma-Aldrich, St. Louis, MO, USA) in order to serve as a loading control (Stouth et al. 2018, Manta et al. 2019, Romero-Calvo et al. 2010). Membranes were washed with 1 x TBST and blocked with 5% milk-TBST or 5% BSA-TBST for one hour before being incubated in a primary antibody overnight at 4 °C with gentle rocking.

We employed antibodies against CARM1 (1:5,000; A300-421A; Bethyl Laboratories, Montgomery, TX, USA), PRMT1 (1:5,000; 07-404; EMD Millipore, Darmstadt, HE, Germany), PRMT5 (1:1,000; 07-405; EMD Millipore, Darmstadt, HE, Germany), MMA (1:1,000; 8015S; Cell Signaling, Danvers, MA, USA), ADMA at glycine and arginine-rich sequences [denoted as $ADMA^{GAR}$ (vanLieshout *et al.* 2019); 1:1,000; 13522; Cell Signaling, Danvers, MA, USA], ADMA-CARM1 motif [denoted as $ADMA\text{-}5^{CARM1}$ (Cheng *et al.* 2018; vanLieshout *et al.* 2019); 1:1,000; another gift from Dr. Mark Bedford, MD Anderson Cancer Center, University of Texas], and SDMA (1:1,000; 13222; Cell Signaling, Danvers, MA, USA) to examine PRMT expression and function. Antibodies against phosphorylated $AMPK^{Thr172}$ (1:1,000; 2535S; Cell Signaling, Danvers, MA, USA), AMPK (1:1,000; 2532S; Cell Signaling, Danvers, MA, USA), phosphorylated ACC^{Ser79} (1:1,000; 3661S; Cell Signaling, Danvers, MA, USA), ACC (1:1,000, 3676S; Cell Signaling, Danvers, MA, USA), PGC-1α (1:200; AB3242; EMD Millipore, Darmstadt, HE, Germany), p53 (1:1,000; 2524S; Cell Signaling, Danvers, MA, USA), and total OXPHOS (1:1,000; ab110413; Abcam, Cambridge, UK) were used to investigate intracellular signalling molecules that regulate the phenotype of skeletal muscle. Antibodies against phosphorylated $ULK1^{Ser555}$ (1:1,000; 5869S; Cell Signaling, Danvers, MA, USA), ULK1 (1:1,000; 8054S; Cell Signaling, Danvers, MA, USA), phosphorylated $FOXO1^{Ser256}$ (1:1,000; 9461S; Cell Signaling, Danvers, MA, USA), FOXO1 (1:1,000; 2880S; Cell Signaling, Danvers, MA, USA), phosphorylated $FOXO3^{Ser588}$ (a kind gift from Dr. Anne Brunet, Department

of Genetics, Stanford University School of Medicine), FOXO3 (1:1,000; 2497S; Cell Signaling, Danvers, MA, USA), p62 (1:1,000; P0067; Sigma-Aldrich, St. Louis, MO, USA), Beclin-1 (1:1,000; 3738S; Cell Signaling, Danvers, MA, USA), TFEB (1:1,000; 4240S; Cell Signaling, Danvers, MA, USA), MuRF1 (1:200; AF5366; R&D Systems, Minneapolis, MN, USA), ubiquitin (1:500; 3933S; Cell Signaling, Danvers, MA, USA), and microtubule-associated protein 1A/1B-light chain 3 (LC3; 1:1,000; 4108S; Cell Signaling, Danvers, MA, USA) were used to identify important markers of the skeletal muscle atrophy program. Antibodies against phosphorylated TBC1D1^{Ser700} (1:1,000; 6929S; Cell Signaling, Danvers, MA, USA) and TBC1D1 (1:1,000; 4629S; Cell Signaling, Danvers, MA, USA) were also employed to assess AMPK activity following acute MK-8722 administration. After overnight incubation in primary antibody, blots were washed with 1 x TBST and incubated in the appropriate secondary antibody (1:2,000; 7074S; Cell Signaling, Danvers, MA, USA) coupled to horseradish peroxidase with gentle rocking at room temperature for one hour. Blots were then washed again with 1 x TBST, followed by visualization with enhanced chemiluminescence (G00069; GE Healthcare Bio-Sciences, Chicago, IL, USA). Blots were developed and analyzed using ImageJ.

Immunoprecipitation (IP)

IP experiments were performed as described previously (Stouth et al. 2018, Philp et al. 2011). Only TA muscles from WT animals were used for IP of CARM1, whereas cohorts of WT and mKO mice were employed for IP of AMPK. For all IP experiments, 200 µg of protein was precleared with 50 µl of protein A agarose suspension (IP02; EMD Millipore, Darmstadt, HE, Germany) and 1 µg of rabbit Immunoglobulin G (IgG; 12-370; EMD Millipore, Darmstadt, HE, Germany). The lysate was mixed by end-over end inversion for 60 minutes at 4 °C followed by centrifugation at 12,000 x g for 10 minutes. Precleared lysate was then rotated by end-over end inversion for 2 hours at 4 °C with either anti-CARM1 (1:100; A300-421A; Bethyl Laboratories, Montgomery, TX, USA) or anti-AMPK (1:100; 2532S; Cell Signaling, Danvers, MA, USA). Next, 50 µl of protein A agarose suspension was added and the samples were mixed by end-over end inversion overnight at 4 °C. The following morning, agarose beads were washed five times with 500 µl of 1 x PBS and centrifugation at 12,000 x g. After suspending each agarose bead complex with equal volumes of 2 x SDS sample buffer (50 µl), samples were boiled for 5 min and centrifuged at 12,000 g for 1 minute. After spinning, only the supernatants were saved for SDS-PAGE (6 µl) separation.

Statistical Analyses

All statistical measures were performed on the raw data sets prior to conversion to the –fold difference values displayed in the graphical summaries. A two-way analysis of variance (ANOVA) was employed to assess the interaction between genotype and muscle for CARM1 mRNA content. A one-way ANOVA was used to evaluate CARM1 protein content in disparate WT muscles. A Student's t test was implemented to assess CARM1 protein content in WT versus mKO heart muscles, as well as to compare body weights and heart weights between genotypes. At each experimental time point in the denervation experiment, a two-way ANOVA was applied to

examine the interaction between genotype and denervation for muscle weight, myofiber CSA, mRNA expression, and protein content. A Student's t test was used to detect differences between DEN and contralateral CON hindlimbs at each time point for CARM1 protein content, as well as the IP experiment of CARM1 in WT mice only. A two-way ANOVA was employed to assess the interaction between genotype and denervation for the IP experiment of AMPK in WT and mKO animals. For the MK-8722 pharmacological study, a two-way ANOVA was also used to examine the interaction between genotype and MK-8722 treatment for mRNA expression and protein content. Tukey post hoc tests were used where appropriate. Data are means ± SEM. Statistical differences were considered significant if $p < 0.05$.

References

Bao, J., Rousseaux, S., Shen, J., Lin, K., Lu, Y. and Bedford, M.T. (2018). The arginine methyltransferase CARM1 represses p300•ACT•CREMτ activity and is required for spermiogenesis. Nucleic Acids Res., 46(9), 4327-4343.

Manta, A., Stouth, D.W., Xhuti, D., Chi, L., Rebalka, I.A., Kalmar, J.M., Hawke, T.J. and Ljubicic, V. (2019). Chronic exercise mitigates disease mechanisms and improves muscle function in myotonic dystrophy type 1 mice. J Physiol., 597(5), 1361-1381.

McCarthy, J.J., Srikuea, R., Kirby, T.J., Peterson, C.A. and Esser, K.A. (2012). Inducible Cre transgenic mouse strain for skeletal muscle-specific gene targeting. Skelet Muscle. 2(1), 8.

Myers, R.W., Guan, H.P., Ehrhart, J., Petrov, A., Prahalada, S., Tozzo, E., Yang, X., Kurtz, M.M., Trujillo, M., Gonzalez, Trotter, D., Feng, D., Xu, S., Eiermann, G., Holahan, M.A., Rubins, D., Conarello, S., Niu, X., Souza, S.C., Miller, C., Liu, J., Lu, K., Feng, W., Li, Y., Painter, R.E., Milligan, J.A., He, H., Liu, F., Ogawa, A., Wisniewski, D., Rohm, R.J., Wang, L., Bunzel, M., Qian, Y., Zhu, W., Wang, H., Bennet, B., LaFranco, Scheuch, L., Fernandez, G.E., Li, C., Klimas, M., Zhou, G., van Heek, M., Biftu, T., Weber, A., Kelley, D.E., Thornberry, N., Erion, M.D., Kemp, D.M. and Sebhat, I.K. (2017). Systemic pan-AMPK activator MK-8722 improves glucose homeostasis but induces cardiac hypertrophy. Science. 357(6350), 507-511.

Philp, A., Chen, A., Lan, D., Meyer, G.A., Murphy, A.N., Knapp, A.E., Olfert, I.M., McCurdy, C.E., Marcotte, G.R., Hogan, M.C., Baar, K. and Schenk, S. (2011). Sirtuin 1 (SIRT1) deacetylase activity is not required for mitochondrial biogenesis or peroxisome proliferator-activated receptor-gamma coactivator-1alpha (PGC-1alpha) deacetylation following endurance exercise. J Biol Chem. 286(35), 30561-70.

Romero-Calvo, I., Ocón, B., Martínez-Moya, P., Suárez, M.D., Zarzuelo, A., Martínez-Augustin, O. and de Medina, F.S. (2010). Reversible Ponceau staining as a loading control alternative to actin in Western blots. Anal Biochem. 401(2), 318-20.

Sacheck, J.M., Hyatt, J.P., Raffaello, A., Jagoe, R.T., Roy, R.R., Edgerton, V.R., Lecker, S.H. and Goldberg, A.L. (2007). Rapid disuse and denervation atrophy involve transcriptional changes similar to those of muscle wasting during systemic diseases. FASEB J., 21(1), 140-55.

Schmittgen, T.D. and Livak, K.J. (2008). Analyzing real-time PCR data by the comparative C(T) method. Nat Protoc. 3(6), 1101-8.

Stouth, D.W., Manta, A. and Ljubicic, V. (2018). Protein arginine methyltransferase expression, localization, and activity during disuse-induced skeletal muscle plasticity. Am J Physiol Cell Physiol., 314(2), C177-C190.

Thomas, M.M., Trajcevski, K.E., Coleman, S.K., Jiang, M., Di Michele, J., O'Neill, H.M., Lally, J.S., Steinberg, G.R., and Hawke, T.J. (2014). Early oxidative shifts in mouse skeletal muscle morphology with high-fat diet consumption do not lead to functional improvements. Physiological reports, 2(9), e12149.

Yadav, N., Lee, J., Kim, J., Shen, J., Hu, M.C., Aldaz, C.M. and Bedford, M.T. (2003). Specific protein methylation defects and gene expression perturbations in coactivator associated arginine methyltransferase 1-deficient mice. Proc Natl Acad Sci USA., 100(11), 6464-8.